JGR Atmospheres

RESEARCH ARTICLE
10.1029/2022JD036618

Impacts of the Desiccation of the Aral Sea on the Central Asian Dust Life-Cycle

Jamie R. Banks[1,2], Bernd Heinold[1], and Kerstin Schepanski[2]

[1]Leibniz Institute for Tropospheric Research (TROPOS), Leipzig, Germany, [2]Institute of Meteorology, Freie Universität Berlin, Berlin, Germany

Key Points:

- The impact of changes in surface water coverage over the Aralkum (the former Aral Sea) for dust emission and transport is investigated
- There is a high degree of interannual variability in the directions of dust-emitting winds over the Aralkum
- Over two thirds of Aralkum dust activity occurs under thick cloud cover, limiting the possibility of it being observed by satellites

Correspondence to:
J. R. Banks,
banks@tropos.de

Citation:
Banks, J. R., Heinold, B., & Schepanski, K. (2022). Impacts of the desiccation of the Aral Sea on the Central Asian dust life-cycle. *Journal of Geophysical Research: Atmospheres*, *127*, e2022JD036618. https://doi.org/10.1029/2022JD036618

Received 10 FEB 2022
Accepted 27 OCT 2022

Author Contributions:
Conceptualization: Jamie R. Banks, Bernd Heinold, Kerstin Schepanski
Data curation: Jamie R. Banks
Formal analysis: Jamie R. Banks
Funding acquisition: Jamie R. Banks
Investigation: Jamie R. Banks
Methodology: Jamie R. Banks, Bernd Heinold, Kerstin Schepanski
Project Administration: Jamie R. Banks
Resources: Bernd Heinold
Software: Jamie R. Banks
Validation: Jamie R. Banks
Visualization: Jamie R. Banks
Writing – original draft: Jamie R. Banks
Writing – review & editing: Bernd Heinold, Kerstin Schepanski

Abstract The formation of the Aralkum (Aral Desert), following the severe desiccation of the former Aral Sea since the 1960s, has created what may be regarded as one of the world's most significant anthropogenic dust sources. In this paper, focusing on dust emission and transport patterns from the Aralkum, the dust life-cycle has been simulated over Central Asia using the aerosol transport model COSMO-MUSCAT (COnsortium for Small-scale MOdelling-MUltiScale Chemistry Aerosol Transport Model), making use of the Global Surface Water data set to take into account the sensitivity to changes in surface water coverage over the region between the 1980s (the "past") and the 2010s (the "present"). Over a case study 1-year period, the simulated dust emissions from the Aralkum region increased from 14.3 to 27.1 Tg year^{-1} between the past and present, an increase driven solely by the changes in the surface water environment. Of these simulated modern emissions, 14.5 Tg are driven by westerly winds, indicating that regions downwind to the east may be worst affected by Aralkum dust. However a high degree of interannual variability in the prevailing surface wind patterns ensures that these transport patterns of Aralkum dust do not occur every year. Frequent cloud cover poses substantial challenges for observations of Central Asian dust: in the Aralkum, over two-thirds of the yearly emissions are emitted under overcast skies, dust which may be impossible to observe using traditional satellite or ground-based passive remote sensing techniques. Furthermore, it is apparent that the pattern of dust transport from the Aralkum under clear-sky conditions is not representative of the pattern under all-sky conditions.

Plain Language Summary Since the 1960s the Central Asian lake that used to be known as the Aral Sea has almost completely dried out, due to human activity. This environmental disaster has created a new desert known as the Aralkum (the "Aral Desert"), which now has a size of 245 km × 245 km across. Dried lakes such as the Aralkum can be very effective sources of wind-driven atmospheric dust. The soils of the Aralkum are also contaminated with agricultural chemicals from nearby croplands, making the Aralkum a major regional threat to human health. Using an atmospheric computer model, we explore the consequences of the new Aralkum for the patterns of atmospheric dust and their potential impacts in Central Asia. We find that the new Aralkum has contributed an extra 7% per year to the total dust quantity over Central Asia, however due to thick cloud cover over two thirds of this dust from the Aralkum cannot be seen by Earth-observing satellites. The wind patterns over the Aralkum vary from year to year, so while our simulations predict that most of the Aralkum's dust is transported to the east during the simulation year, during other years plenty more dust will be transported elsewhere.

1. Introduction

Changes in dust storm activity within the Earth's atmosphere may be driven on the decadal timescale by changes in climate and/or by changes in land surface properties. One mechanism driving enhanced dust activity is the desertification of vegetated and agricultural land, which exposes an increased area of bare soil to wind erosion. Similarly, the desiccation of former lakes expands the land surface area, exposing potentially highly erodible lakebeds (e.g., Gillette et al., 2004, and others). The classic example of a dust-producing dry lakebed is the Bodélé Depression in the Sahara Desert in Chad (e.g., Todd et al., 2007; Washington et al., 2006), which was formed millennia ago by the desiccation of Mega-Lake Chad (Gasse, 2002), and which is now recognized to be the pre-eminent single dust source in the world (e.g., Koren et al., 2006, and others). Meanwhile the pre-eminent example of a lakebed dust source that has been formed during the past century is the former Aral Sea, on the border between Kazakhstan and Uzbekistan in Central Asia.

1.1. The Aralkum, the Desert of the Former Aral Sea

Up until the early 1960s the Aral Sea was the fourth largest lake in the world (Breckle & Geldeyeva, 2012), with a surface area of ~68,000 km^2, and was able to sustain a significant fishing industry (Micklin, 2010). A terminal lake, it is supplied by the Amu Darya and the Syr Darya rivers which flow from the south and east, from the Pamir and the Tian Shan mountains. In the early 1960s the water flow from these two rivers and their tributaries was more aggressively diverted for irrigation, reducing substantially the eventual water discharge into the Aral Sea. This triggered the catastrophic shrinkage of the Aral Sea over a timescale of decades, and by 2009 it had reduced in area by approximately 90% compared to its value in 1960 (Micklin, 2010), coupled with a dramatic increase in the salinity of the remaining Sea. In ~1990 the "North Aral Sea" became disconnected from the rest of the Sea (Shi et al., 2014), and was subsequently dammed off by Kazakhstan, as a result of which its area and volume has become relatively stable in recent decades, and its water quality has seen some recovery. In contrast, the less-protected southern part of the Sea has seen continued deterioration and has become subdivided into a western and an eastern lobe: the western lobe of the South Aral Sea is deeper and narrower than the eastern lobe, which exhibits a larger degree of interannual variability in its surface area, a variability which is governed primarily by the variability in water discharge to the Sea. Given this dramatic reduction in the surface area of the Aral Sea, leaving behind over 60,000 km^2 of barren former lakebed susceptible to wind erosion, it is now perhaps more appropriate to refer to the Aral Sea region instead as the "Aralkum," the "Aral Desert" (Breckle & Wucherer, 2012). The scale of the deterioration of the Sea between the 1980s and the 2010s is depicted by the two satellite images in Figure 1.

As a consequence of this desiccation, over the past few decades the Aralkum has become another source of desert dust aerosol (e.g., Groll et al., 2013; Nobakht et al., 2021, and others) within the arid Central Asian region (see map in Figure 2), joining older deserts such as the Karakum (~350,000 km^2) to the south in Turkmenistan and the Kyzylkum (~300,000 km^2) to the south-east in Uzbekistan and Kazakhstan. Due to the cause of its formation, dust from the Aralkum may be regarded as anthropogenic in origin, in contrast to the natural origins of dust from the Sahara or from the Karakum for example, and so we may see it as a marker of human-induced environmental change. Compared to typical natural dust sources the Aralkum has the extra and undesirable characteristic that the soils of the Aralkum are polluted with fertilisers and pesticides from the irrigation systems connected to the Amu Darya and Syr Darya rivers, exacerbating the health hazards posed by dust from the Aralkum region (O'Hara et al., 2000; Sternberg & Edwards, 2017; Wiggs et al., 2003).

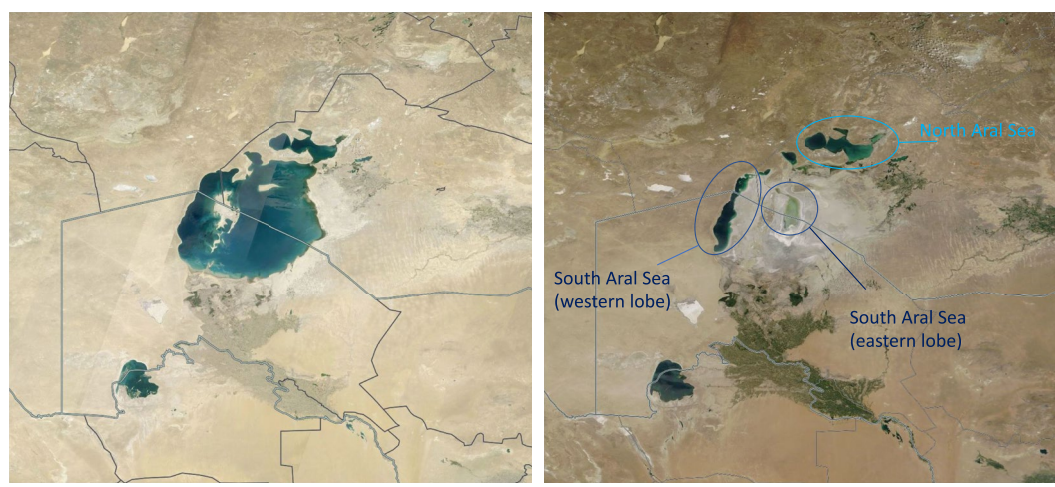

Figure 1. True color satellite images of the Aral Sea taken three decades apart, as a composite by Landsat during 1986 (left), and by Terra MODIS (Moderate Resolution Imaging Spectroradiometer) on 28 July 2015 (right). The boxes have bounds 40°–49°N, 55°–65°E. In the southern part of the Sea, the maximum width in the 1980s was ~220 km; by the 2010s, the maximum width of the western lobe of the South Aral Sea was ~30 km. Images obtained 24 November 2021 and 2 August 2022 from https://worldview.earthdata.nasa.gov.

Figure 2. Map of the Central Asian and Middle Eastern region considered in this paper, overlaid on the NASA "Blue Marble" image. Selected relevant national capital cities are marked by red star symbols and numbered as follows: (1) Ashgabat, Turkmenistan; (2) Baku, Azerbaijan; (3) Dushanbe, Tajikistan; (4) Kabul, Afghanistan; (5) Tashkent, Uzbekistan; (6) Tehran, Iran. Relevant drying lakes and deserts are also labeled. The orange stars refer to the deposition-relevant locations in Section 4.4: (1) the Kazakh town of Kazaly; (2) the Uzbek city of Nukus; (3) the Pamir-Alay mountains in Tajikistan.

1.2. Current Scientific Understanding of Aralkum Dust Activity

The patterns of dust activity from the newly-formed Aralkum have drawn increasing research attention over the past two to three decades. On the ground, research studies have taken the form of wind-tunnel experiments on the dust emission properties of the Aralkum's soils (Argaman et al., 2006) and measurements of dust deposition (Groll et al., 2013, 2021; Opp et al., 2017, 2019) at regional sites near the Aralkum. Sampling various soils characteristic of the southern Aralkum in Uzbekistan, Argaman et al. (2006) identified fine-grained Takyr soils (common to Central Asia) as having particularly low threshold friction velocities, and which hence have a high potential for dust emission. Dust deposition measurements have been made in the region since at least 2003, as reported by Groll et al. (2013), with up to 23 sites distributed to the south and east of the Aralkum across Kazakhstan, Uzbekistan, and Turkmenistan (Groll et al., 2021). These measurements highlight not just the significance of the Aralkum's dust within the region, but also highlight the likely dominance of the Kyzylkum to the regional dust loading. These authors also performed mineralogical and size analyses on the deposited dust samples.

Meanwhile the larger regional view over the Aralkum has been informed by the analysis of satellite observations and retrievals (e.g., Löw et al., 2013; Rupakheti et al., 2019). Analyses of National Oceanic and Atmospheric Administration, Advanced Very-High-Resolution Radiometer (NOAA AVHRR) satellite imagery performed by Indoitu et al. (2015) using data from 2005 to 2008 identified between six and nine dust storm events per year being emitted from the Aralkum; the same authors also use Ozone Monitoring Instrument (OMI) Aerosol Index (AI) retrievals to indicate that the most frequent dust events from the Aralkum during this period were emitted toward the west, although the authors do note a change toward the east later during the analysis period. Ge et al. (2016) also analyzed OMI AI data over the Aral Sea region to calculate a persistent increase in the yearly average AI of ~50% between 2005 and 2013, signifying the growing presence of the Aralkum as a Central Asian dust source. More recently Nobakht et al. (2021) made use of MODIS satellite data from 2003 to 2012 to compile an inventory of dust emission point sources over Central Asia and western China, highlighting the Aralkum as one of the major regional dust sources, with particularly high densities of point sources in the eastern and southern portions of the Aralkum basin. These are the oldest and driest portions of the Aralkum, which were the first areas of the lakebed to be exposed during the 20th century.

The recent formation of the Aralkum has also posed challenges for modeling systems, for example, due to its changing water coverage and its uncertain soil properties, hence in order to address this a number of dust modeling studies have been performed for the Aralkum and Central Asia in recent years. This has generally required the land use properties used by models, for example, the Weather Research and Forecasting (WRF) model (e.g., Darmenova et al., 2009; Darmenova & Sokolik, 2007; Li & Sokolik, 2017; Xi & Sokolik, 2016b), to be updated to include the dry and barren features of the new Aralkum. It is often the case that the default data sets used by models (e.g., for land use types and soil properties) assume that the original Aral Sea water coverage is still valid in the modern era, which would prevent simulations of dust emissions from the new Aralkum. Building on previous WRF model development and focusing on the regional Central Asian scale, Xi and Sokolik (2016a) performed simulations from 2000 to 2014 and observed a negative trend in regional dust emissions (per unit area within Central Asia) due to decreasing strong wind events, which the authors attribute to changes in the large-scale atmospheric circulation patterns. Li and Sokolik (2018) subsequently made use of these simulations to make estimates of the dust direct radiative effect over Central Asia. A more recent study by Karami et al. (2021), comparing the performance of three models (including WRF-Chem) with MODIS satellite aerosol retrievals during case studies of Central Asian dust events including from the Aralkum, found that all of the models underestimated the dust loadings close to the source regions. The Aralkum and desiccating lakes in the region remain challenges for model representations of the Central Asian dust life-cycle.

1.3. Other Desiccating Lakes in Central Asia and the Middle East

The Aral Sea is not the only lake in Central Asia and the Middle East which has undergone devastating desiccation over the past few decades. Lake Urmia is a lake in north-western Iran (see Figure 2), near the Turkish border, which has been reported by Tourian et al. (2015) to have lost ∼70% of its area between 2002 and 2014, with a reduction in water volume from 10 to under 2 km^3 during this period. This has been caused by water mismanagement and by drought, and has led to the lake having the potential to be a local dust source (Abadi et al., 2022; Gholampour et al., 2015; Sotoudeheian et al., 2016). In more recent years it has, however, seen some positive recovery in its water coverage. An even more substantial dust source is the Hamoun Lake situated further east in the Sistan Basin straddling the border between Iran and Afghanistan (e.g., Rashki et al., 2013; Sharifikia, 2013), which has become a dust source due to prolonged drought in the region. The Sistan Basin is also subject to the Levar wind, the "Wind of 120 Days", a persistently strong summertime wind system along the Iran-Afghanistan border which is a significant trigger for dust activity in the region (e.g., Alizadeh-Choubari et al., 2014; Kaskaoutis et al., 2015).

This paper seeks to explore two main questions about dust emitted from the Aralkum and other desiccating lakes in Central Asia. First, what are the consequences of this desiccation of numerous lakes in the region for regional dust activity? Furthermore, how extensive, in space and time, is the "sphere of influence" of the Aralkum and of the other dry lakebed dust sources? And second, to what extent can these changes in dust activity be measurable, for example, in retrievals by satellite instruments? We will explore these questions using the regional dust transport model COSMO-MUSCAT (COSMO: COnsortium for Small-scale MOdelling; MUSCAT: MUlti-Scale Chemistry Aerosol Transport Model), which we will describe in Section 2, along with the updates to the assumed surface soil and water properties that we have implemented in order to simulate dust emission over the Central Asian region. In Section 3 we describe the meteorological situation in Central Asia during the simulated year, considering also the interannual variability in wind patterns over the Aralkum, before describing the simulated dust emission patterns from the Aralkum and the wider Central Asian region. In Sections 4.1 and 4.2 we compare the COSMO-MUSCAT simulations with ground-based and satellite observations, and with the Copernicus Atmosphere Monitoring Service (CAMS) aerosol reanalysis data set, both over the course of the year and for specific Aralkum dust events. Finally, in Sections 4.3 and 4.4 we describe the geographical range of dust transported from the Aralkum, along with its regional deposition patterns.

2. Modeling Strategy: The COSMO-MUSCAT Model and the "Dustbelt" Domain

2.1. The COSMO-MUSCAT Model

The COSMO-MUSCAT atmosphere-dust model is comprised of the online coupling of version 5.05 of the non-hydrostatic atmospheric model COSMO (Schättler et al., 2014) with the chemistry tracer transport model MUSCAT (Wolke et al., 2012), and is used to simulate the emissions, atmospheric concentrations and radiative effects of dust aerosols (Heinold et al., 2011). Dust is subject to emission and dry and wet deposition processes, and is treated as a passive tracer in five size bins ranging in radii from 0.1 to 24.0 μm. The particles are assumed to be spherical and to have a mineral density of 2.65 g cm^{-3} (i.e., that of quartz).

Within the COSMO-MUSCAT aerosol transport modeling system airborne dust is simulated to interact with radiation (Helmert et al., 2007), and radiative feedback is included in order to simulate the dust impact on the atmospheric dynamics. The dust aerosol optical depth (DOD) is calculated at 550 nm based on extinction efficiencies Q_{ext} derived using Mie theory (Mie, 1908) and dust refractive indices described by Sinyuk et al. (2003). See Schepanski et al. (2017) and Banks et al. (2018) for further details and discussion on the utility and capabilities of COSMO-MUSCAT for simulations of dust transport and satellite observations over North Africa.

In order to efficiently simulate not only dust from Central Asia and the Middle East, but also the large quantities of dust that can be advected over from the neighboring Sahara, a rectangular rotated pole grid has been chosen for the COSMO-MUSCAT simulation domain which has a grid spacing of 28 km, that is, 0.25°. This spatial grid is referred to as the "Dustbelt," abbreviated to "DUBLT." The origin of the rotated grid is located at 20°N, 45°E, in southern Saudi Arabia: the corresponding North Pole longitude of the grid is at −135°, the North Pole latitude is at 70°. The latitude in the rotated pole grid ranges from −10° to 30°, while the longitude ranges from −60° to 30° (160 × 360 grid cells): rotated back into geographical coordinates the domain is bounded in latitude by ∼0° and 50°N, and in longitude by ∼28°W and 84°E. The domain therefore covers the North African Sahara,

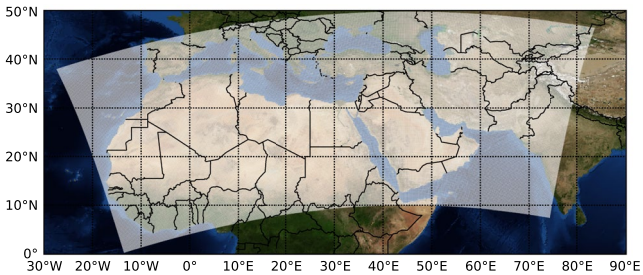

Figure 3. Map of the Dustbelt domain, shaded in white.

southern Europe, the Middle East, and Central Asia as far east as western India and western China, as shown in Figure 3. Initial and boundary wind data for COSMO come from the global re-analysis of the weather forecast model ICON (Zängl et al., 2015), which has been operational at the German weather service (Deutscher Wetterdienst, DWD) since 2015, and has a grid spacing of 13 km.

2.2. Dust Emission Parameterization

Dust emission is simulated following the saltation bombardment parameterization scheme developed by Marticorena and Bergametti (1995), whereby the vertical dust emission flux F is described by a linear relationship with the horizontal saltation flux G. It is implemented in COSMO-MUSCAT as described by Tegen et al. (2002). Dust may only be emitted from the surface when the wind friction velocity u_* is greater than the threshold friction velocity $u_{*,\mathrm{t}}$ of the surface, a property which is dependent on surface properties such as the aerodynamic aeolian roughness length z_0 (e.g., Menut et al., 2013, and others), vegetation cover, and the soil size distribution. The horizontal saltation flux is a function of particle diameter D_p and is described by the equation:

$$G = \frac{\rho_{\mathrm{a}}}{g} u_*^3 \sum_i \left[\left(1 + \frac{u_{*,\mathrm{t}}\left(D_{\mathrm{p}_i}\right)}{u_*} \right) \left(1 - \frac{u_{*,\mathrm{t}}^2\left(D_{\mathrm{p}_i}\right)}{u_*^2} \right) \right] s_{\mathrm{i}}, \tag{1}$$

where s_i is the fraction of the dust size bin i present in the soil, ρ_a is the air density, and g is the Earth's gravity.

The calculation of the emitted dust fluxes is driven by the wind fields and ambient meteorology that are passed from COSMO to MUSCAT. Where and when the daily accumulated precipitation exceeds 2.5 mm, dust emissions are suppressed completely. As in other state-of-the-art dust models (e.g., Cakmur et al., 2004; Lunt & Valdes, 2002; Morcrette et al., 2008), COSMO-MUSCAT also considers gusts in its latest version. In order to account for the sub-gridscale variability in the surface wind speeds during a time-step, the maximum wind speed derived from a calculation of the turbulent and convective gusts (Schulz & Heise, 2003) are considered in addition to the grid-scale wind speed. Winds therefore have two components within the dust emission scheme, the bottom layer grid-scale wind speed for 100 s and the gust diagnostic for a duration that characteristically lasts up to 20 s (American Meteorological Society, 2022). This is a new feature of the DUBLT dust modeling strategy within the COSMO-MUSCAT model.

The suppression of dust emission by snow cover is characterized by the fractional snow cover A_{snow}, with dust emissions being multiplied by a factor of $(1 - A_{\mathrm{snow}})$ in the presence of snow. NASA Aqua MODIS 8-day snow cover fields are used for this purpose (Hall & Riggs, 2016). Similarly, dust is suppressed by vegetation cover as represented by the fraction of photosynthetically active radiation (FPAR: Knorr & Heimann, 1995), derived from monthly Aqua MODIS NDVI (normalized difference vegetation index) retrievals (Didan, 2015):

$$FPAR = 1.222 \left(\frac{NDVI}{0.559} - 0.1566 \right). \tag{2}$$

As described by Tegen et al. (2002), the monthly FPAR value is used to calculate a monthly effective surface area fraction A_{eff} of bare soil, by relating the FPAR value to the biome type (Kaplan, 2001) of the grid cell.

Collating these pieces of information along with the land fraction A_{land}, the vertical emission flux F is derived from the saltation flux G via the relationship:

$$F = \alpha * (1 - A_{\mathrm{snow}}) * A_{\mathrm{eff}} * A_{\mathrm{land}} * G. \tag{3}$$

α is the "sand-blasting efficiency" (units cm^{-1}) and is a property which is dependent on the soil particle size distribution. Following Marticorena et al. (1997) and Tegen et al. (2002) α is estimated using the following relationship based on the clay, silt, and sand contents of the soil:

$$\begin{aligned} \alpha = 0.01 * \Big(\left(\%clay * \alpha_{\mathrm{clay}} \right) + \left(\%silt * 10^{-5} \right) + \\ \left(\%sand_{\mathrm{medium/fine}} * 10^{-6} \right) + \left(\%sand_{\mathrm{coarse}} * 10^{-7} \right) \Big), \end{aligned} \tag{4}$$

where $\alpha_{clay} = 10^{-6}$ for a clay content of <45% and 10^{-7} for a clay content of >45%.

2.3. Assumed Surface Properties

Surface properties are determined by external data sources. The surface aerodynamic roughness length z_0 is retrieved from ASCAT and PARASOL satellite measurements as carried out by Prigent et al. (2012). These data are provided on a 0.125° regular grid and are then re-gridded onto the 0.25° DUBLT rotated grid. Within the DUBLT domain the maximum grid-cell value of z_0 is 2.31 cm, with water, ice and other non-retrievable surfaces being given a value of 0 cm over which emission flux calculations are not attempted. Non-retrieved surfaces include the Aralkum, perhaps due to the assumed land-sea mask, or due to the variations in water coverage over the retrieval period.

One of the most substantial changes in the COSMO-MUSCAT dust emission and transport scheme which has been introduced within the scope of the DUBLT modeling strategy compared to previous model versions described by Heinold et al. (2011) and Schepanski et al. (2017) concerns the soil size distribution, which is now defined by version 2.0 of the SoilGrids250m data set (Poggio et al., 2021), released in May 2020 as an update to the SoilGrids data set described by Hengl et al. (2017). SoilGrids is a project of the International Soil Reference Information Centre to automate the creation of a globally consistent soil database. This provides the clay, silt and sand percentages of the soil on a Homolosine global projection, with a resolution of up to 250 m but also downloadable at coarser resolutions. The database was created using ~240,000 soil profiles from around the world, merged onto a global grid using machine learning techniques, with the clay, silt and sand percentages transformed using the additive log ratio transformation. It is important to note that, as Poggio et al. (2021) point out, while in Europe there is a relatively high density of profiles (~ four profiles per 10 km^2) in countries such as Kazakhstan there may only be less than one profile per 10 km^2, due to physical remoteness and/or the fact that some soil profile data sets may not be shared. These difficulties are even more pronounced in the new Aralkum, where there are no available SoilGrids data. It is therefore to be expected that the SoilGrids data will have higher uncertainties in remote regions of the Dustbelt compared to over Europe and North America.

For the purposes of the DUBLT simulations the soil properties chosen are the mean values from the uppermost layer of the soil profiles. The soil texture of each SoilGrids point is derived by sorting these clay, silt and sand percentages into the soil textural triangle as defined by the US Department of Agriculture (Soil Science Division Staff, 2017), which specifies 12 soil textures: clay, silty clay, sandy clay, clay loam, silty clay loam, sandy clay loam, loam, silt loam, sandy loam, silt, loamy sand, and sand. A thirteenth non-soil "soil texture" is considered within the model domain and represents non-soil surfaces such as water and ice. Within the SoilGrids data set there are masks for glaciers and bare rock (Hengl et al., 2017). Transforming the SoilGrids data points to the 28 km-resolution DUBLT domain, a fraction of each of the 13 soil textures is assigned to each DUBLT grid cell. Previous COSMO-MUSCAT dust model versions had only one dominant soil type per grid cell. These fractions of the 13 soil textures are re-normalized so as to exclude the water fractions, which are accounted for by the use of the land-water mask described in the next paragraph. Further to this, for each soil texture within each DUBLT grid cell an average value of the clay, silt and sand percentages is calculated from all of the SoilGrids points within that DUBLT grid cell with that soil texture. These average clay, silt and sand values per soil texture are then used to calculate the α value per soil texture and per grid cell, with emission fluxes being calculated for each soil texture and then integrated by the soil texture fraction to obtain the overall grid cell dust emission flux.

The other major change introduced by the DUBLT modeling strategy to the COSMO-MUSCAT dust emission scheme concerns the treatment of the surface water coverage, which requires a more dynamic surface water data set compared to the more static treatment allowable over the Sahara. The creation of new lakebed dust sources is defined within the DUBLT domain using surface water coverage changes provided by the Global Surface Water data set (Pekel et al., 2016) provided by the European Commission's Joint Research Centre within the context of the Copernicus Programme. These data are publicly available at https://global-surface-water.appspot.com/ (last accessed 9 September 2022). The data set tracks global surface water changes between 1984 and 2015 using Landsat satellite images, at a resolution of 30 m. Merging this high resolution data onto the DUBLT domain, the gridded fractional surface water coverage is obtained for the 1980s and the 1990s (1984–1999, the "past" epoch) and for the 2000s and the 2010s (2000–2015, the "present" epoch). The "seasonality" of a pixel within each grid cell is also accounted for, as a temporal average over the year. Maps of the past and present water coverage, and

their difference, are presented in Figure 4 for the Central Asian region (considered for the purposes of this study to be bound by 29°–49°N, 44°–72°E) in order to focus on the major potential lakebed dust sources in the region.

Potential new lakebed dust sources may be identified by considering the difference between the present land fraction and the past land fraction. This identifies predominantly the Aralkum as a potential lakebed dust source within the region, but also identified are the Sistan Basin and Lake Urmia. The re-filling of the Garabogazköl Basin lagoon on Turkmenistan's Caspian Sea coast after a dam breach in 1992 (Pekel et al., 2016), having been dry for several years during the 1980s, is clearly noticeable in Figure 4c as being the major contrasting example in the region of an area that has seen an increase in water coverage, and hence may be considered to be a potential "past" lakebed dust source. The changes in land area in the three decades between the past and the present is estimated to be +25,371 km^2 for the Aralkum, +871 km^2 for the Sistan Basin, +1,671 km^2 for Lake Urmia, and −14,450 km^2 for the Garabogazköl Basin. The value of +25,371 km^2 for the Aralkum is rather less than the ∼60,000 km^2 of lake that has been lost since it started to dry out in the early 1960s, indicative of the extent of the desiccation of the Aral Sea that had already occurred by the end of the 1980s and the 1990s.

As indicated previously, the surface properties of the new Aralkum are only sparsely described by the soil and roughness length databases, a challenge which is partially due to its relatively recent formation and its inaccessibility to field researchers, but may also be influenced by the difficulties posed to satellite retrievals for example, by temporally varying water coverage. Given this paucity of consistent data coverage over the Aralkum, assumptions as to the surface properties are required in order to simulate dust emissions from the Aralkum and from other new potential dust sources opened up by drying lakes. Given the often smooth nature of lakebed surfaces constant roughness lengths are applied to their surfaces based on the minimum values retrieved by Prigent et al. (2012) in the immediate vicinity of their basins. So for example, missing grid cells within the new Aralkum are given a constant z_0 of 0.020 cm, while the Garabogazköl Basin and Lake Urmia are given values of 0.026 and 0.054 cm. SoilGrids data are also missing in the centre of the old Aral Sea, as well as the Garabogazköl Basin and parts of Lake Sarygamysh (on the Turkmen-Uzbek border), and so in order to make estimates of past and present dust emissions in these regions the soil properties are replaced by soil measurements taken by Argaman et al. (2006) in the Amu Darya delta region of the southern Aralkum in Uzbekistan. These are acquired from an averaging of the size distributions measured at the two sampling sites (6 and 7) which were considered by the authors to be "exposed Aral Sea bottom sediments", desiccated between the mid-1980s and the mid-2000s, and are displayed in Table I of Argaman et al. (2006). Within the DUBLT modeling scenarios, this leads to a silty loam soil with 11.56% clay, 55.44% silt, and 33% clay.

An important caveat to mention here is that the influence of potentially salt-encrusted lakebed sediments is currently omitted in the Aralkum (and other lakebed) dust emission simulations. It is known that lakebed soils and dust can be highly saline (e.g., Gholampour et al., 2015, and others), including from Lake Urmia and the Aralkum, and that this may affect the conditions under which dust can be emitted from these sources (Buck et al., 2011). An important consideration in this regard would be the degree of disturbance of the soil surface (Nield et al., 2016), which can vary by temperature and soil moisture, and hence may display a dependence on the time-of-day and the season as well as on the local climatic conditions. An improved representation of dust emissions from salty lakebeds in future generations of the COSMO-MUSCAT modeling system (and in other models) would require more robust parameterisations of these processes. Focusing on the Aralkum specifically, the wind tunnel experiments performed by Argaman et al. (2006) indicated that salt-crusted Solonchak soils had higher threshold friction velocities than Takyr soils, soils that are also saline but which are also characteristic of the Central Asian deserts: this finding therefore implies that Takyr soils are more susceptible to wind erosion than Solonchaks. As can be seen in Figure 16 of Indoitu et al. (2015), Solonchaks are present predominantly in the more recently-dried centre of the Aralkum, while the Takyrs are prevalent in the older surrounding areas. The distinction between these two types of soils is not made in the current DUBLT Aralkum simulations, and may lead to over-estimated dust emissions over Solonchak soils in particular.

2.4. Modeling Scenarios

Three scenarios are defined, as experiments to explore the consequences of desiccating lakes for dust activity in the region: "DUBLT," "DUBLT_PAST," and "DUBLT_ARAL." The primary scenario is the DUBLT scenario, using present day surface water coverage and simulating potential dust sources throughout the Dustbelt. Similarly, DUBLT_PAST simulates Dustbelt dust emissions using the surface water coverage from the past epoch,

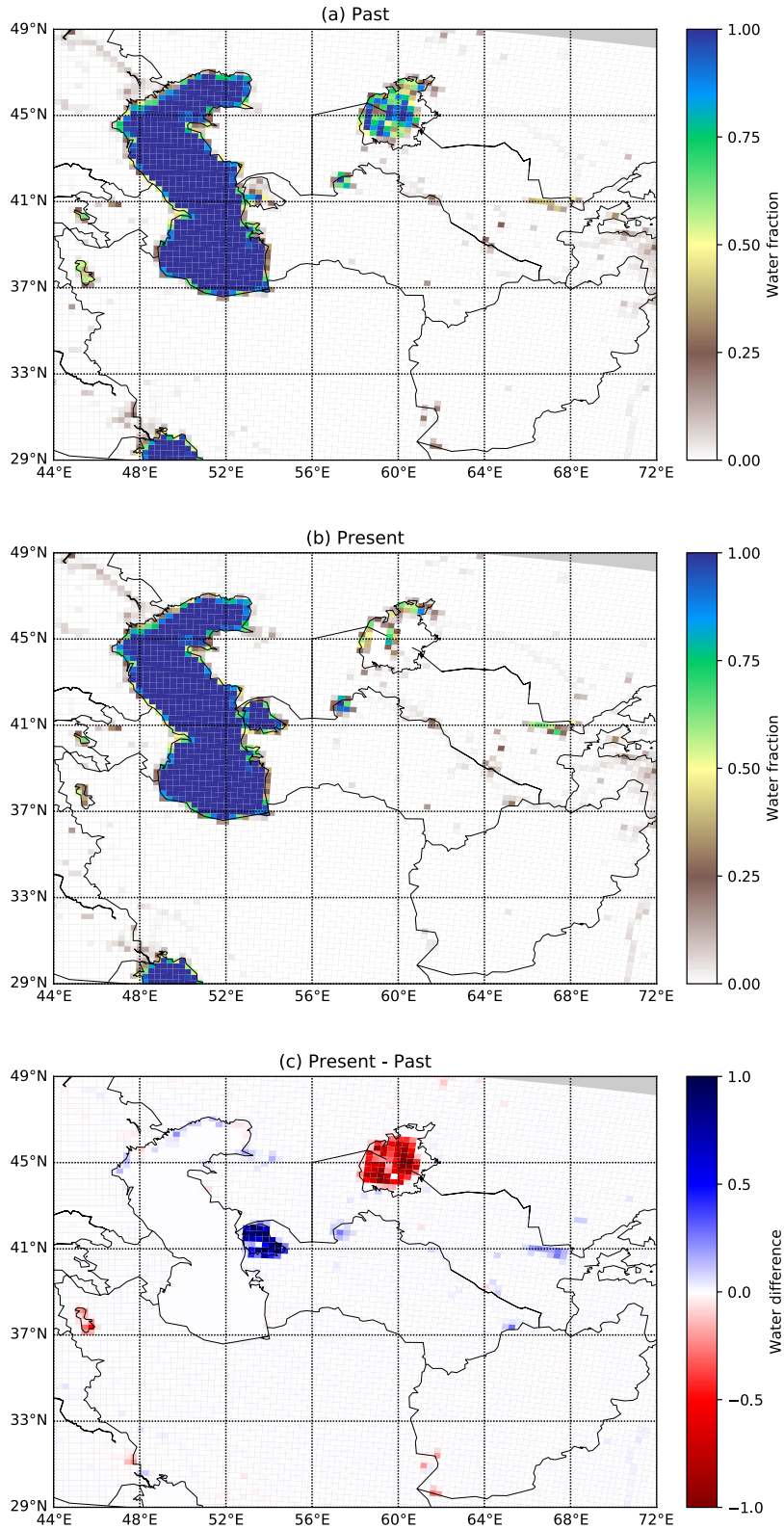

Figure 4. Maps of surface water coverage gridded onto the Central Asian domain, for (a) the 1980s and the 1990s ("past"), (b) the 2000s and the 2010s ("present"), and (c) present - past water coverage.

during the 1980s–1990s. Finally as a sensitivity study, DUBLT_ARAL simulates only dust emission from the Aralkum lakebed region in the present, in order to isolate the effect of Aralkum dust. Each scenario is modeled for a one-year time period, chosen to be from March 2015 to March 2016: this period is contemporaneous with the present-era water coverage, and with the establishment of a ground-based lidar system at Dushanbe, Tajikistan (Hofer et al., 2017, 2020). The precise date range is the 366-day year from 30 March 2015 to 29 March 2016. In considering the same year for all three scenarios, the aim is to understand the changes in the regional dust life-cycle solely due to the changes in surface water coverage between epochs, while maintaining consistent atmospheric conditions between the three experiments.

3. Dust Emissions From the Aralkum and Central Asia

3.1. The Meteorological Situation in Central Asia, on the Seasonal and Interannual Timescale

In order to understand dust activity from the Aralkum, it is instructive first to consider the meteorological conditions which drive it. Figure 5 describes the simulated pressure and wind fields which drive dust activity over the Aralkum in the present-era DUBLT model run, compared to the seasonal mean conditions. Seasonally the strongest mean winds over the Aralkum and the Central Asian deserts are in summer, characterized by northerly winds heading southwards toward a frequent low pressure system over southern Afghanistan. This is the wind system that when funneled between the mountains on the Afghan-Iranian border gives rise to the Levar wind and regionally intense dust emissions; that this is associated with an anticyclone over the Caspian Sea is consistent with the findings of Kaskaoutis et al. (2015), who used National Centers for Environmental Prediction (NCEP) reanalysis data to note how this enhances the longitudinal pressure gradient. The summer Aralkum dust cases also arise when the pressure gradients intensify, accentuating the prevailing northerly wind pattern to produce dust events which would typically head south- and south-eastwards. In contrast, the spring and winter Aralkum dust events are characterized by low pressure regimes to the north, over Kazakhstan and Russia, generating westerly winds which would emit Aralkum dust in the eastwards direction.

There is however a large degree of interannual variability in the wind patterns over the Aralkum, as described by the directional surface wind distributions in Figure 6, derived from ERA5 reanalysis data (Hersbach et al., 2018, 2020) over a 15-year period up to 2020. The 2015–2016 period appears to be something of an outlier in the strength of its westerly and south-westerly winds, notably higher than almost every other year with the exception of 2007. In contrast the easterly and north-easterly winds during the 2015–2016 period are comparatively weak compared to the average, indicating the potential for dust events from these directions to occur in previous years but not during the DUBLT simulation period. Overall though, the 2015–2016 period is marked by a greater frequency of stronger wind events compared to the average (again with the exception of 2007), indicating the potential for this to have been a particularly dusty year for the Aralkum and that an “average” year may have smaller dust emissions.

It is therefore clear that this interannual variability in the directions of the dust-emitting wind speeds will have implications for the year-to-year patterns in dust emission from the Aralkum. Simply by considering the ERA5 directional wind speed distributions, we may infer that 2007 may have been a particularly dusty year overall for the Aralkum, driven especially by westerly and north-westerly winds. Northerly winds may have been responsible for intense dust storms in 2018, while dust storms driven by southerly winds may have been intense in 2006: these intense southerly winds have been highlighted by Opp et al. (2019), who also noted that southerly winds became less frequent over the region in later years, and this observation is borne out by the wind distributions for the later years in panel (h). More recently, 2019 appears to have been a year with a more familiar easterly and north-easterly wind pattern, with high potential for intense dust storms driven by these winds. The Aralkum therefore appears to be a desert dust source which is particularly sensitive to the meteorological situation over Central Asia in a given year, highlighting also the substantial uncertainties in our knowledge of the Aralkum's dust emission patterns on a longer timescale.

Expanding on the DUBLT year's place in the context of interannual variability, Figure 7 depicts the monthly total precipitations and mean snow covers for the DUBLT year and the years within the 2006–2020 period. In terms of precipitation, the Aralkum is in general a fairly arid environment but with more precipitation in spring and winter. During the DUBLT year, April–May 2015 were quite wet, followed by a slightly below-average summer. 2015 ended with a comparatively very wet November and December, and was followed by March 2016

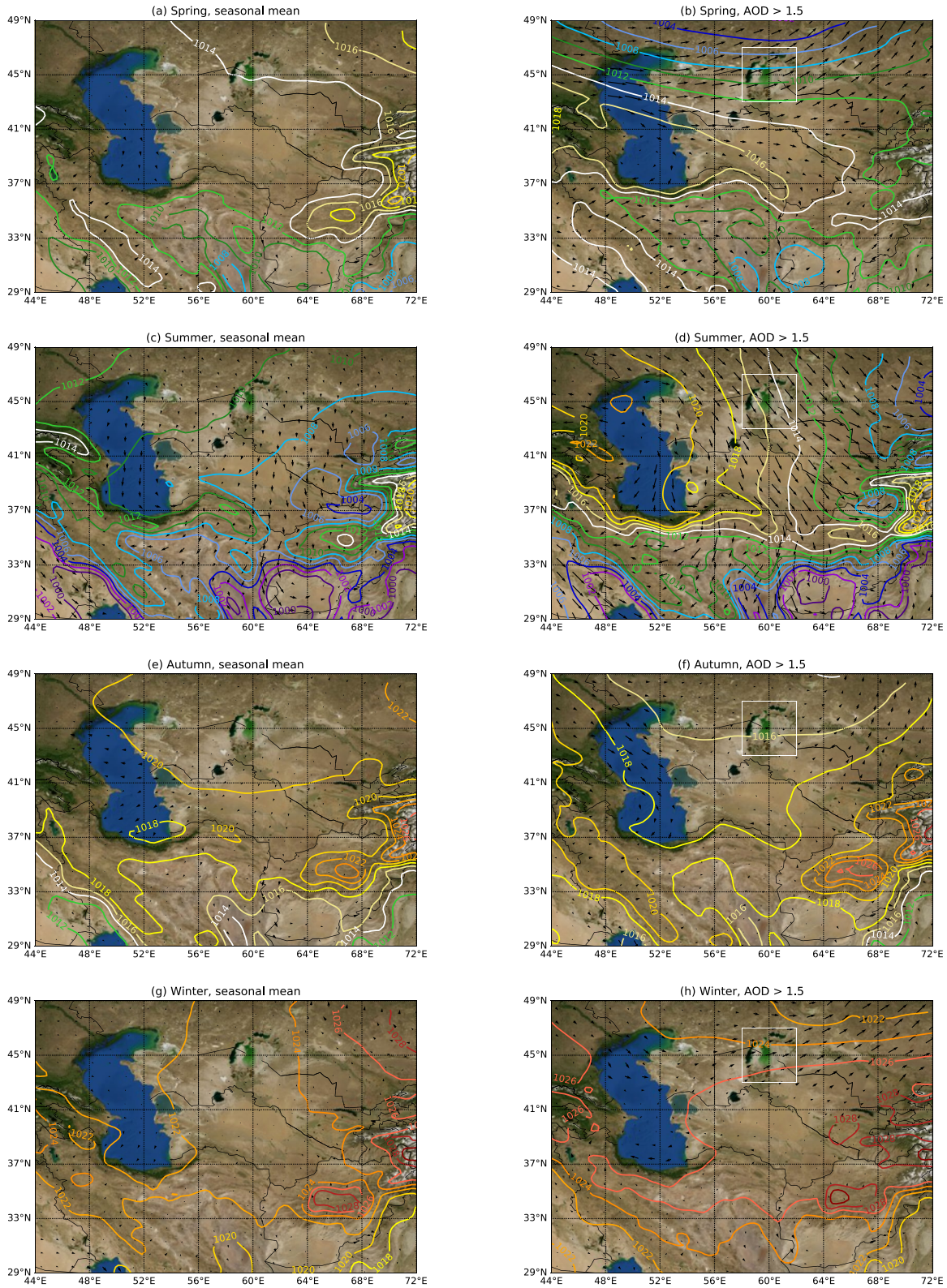

Figure 5. Seasonal mean pressure at mean sea level (colored contour lines, 2 hPa intervals) as simulated by the DUBLT scenario (left column), and composited by timeslots when the maximum dust aerosol optical depth (DOD) within the white Aralkum box is >1.5 (right column). The wind arrows are normalized to the same scale, with peak mean wind speeds of 12.2 m s^{-1} in panel (d).

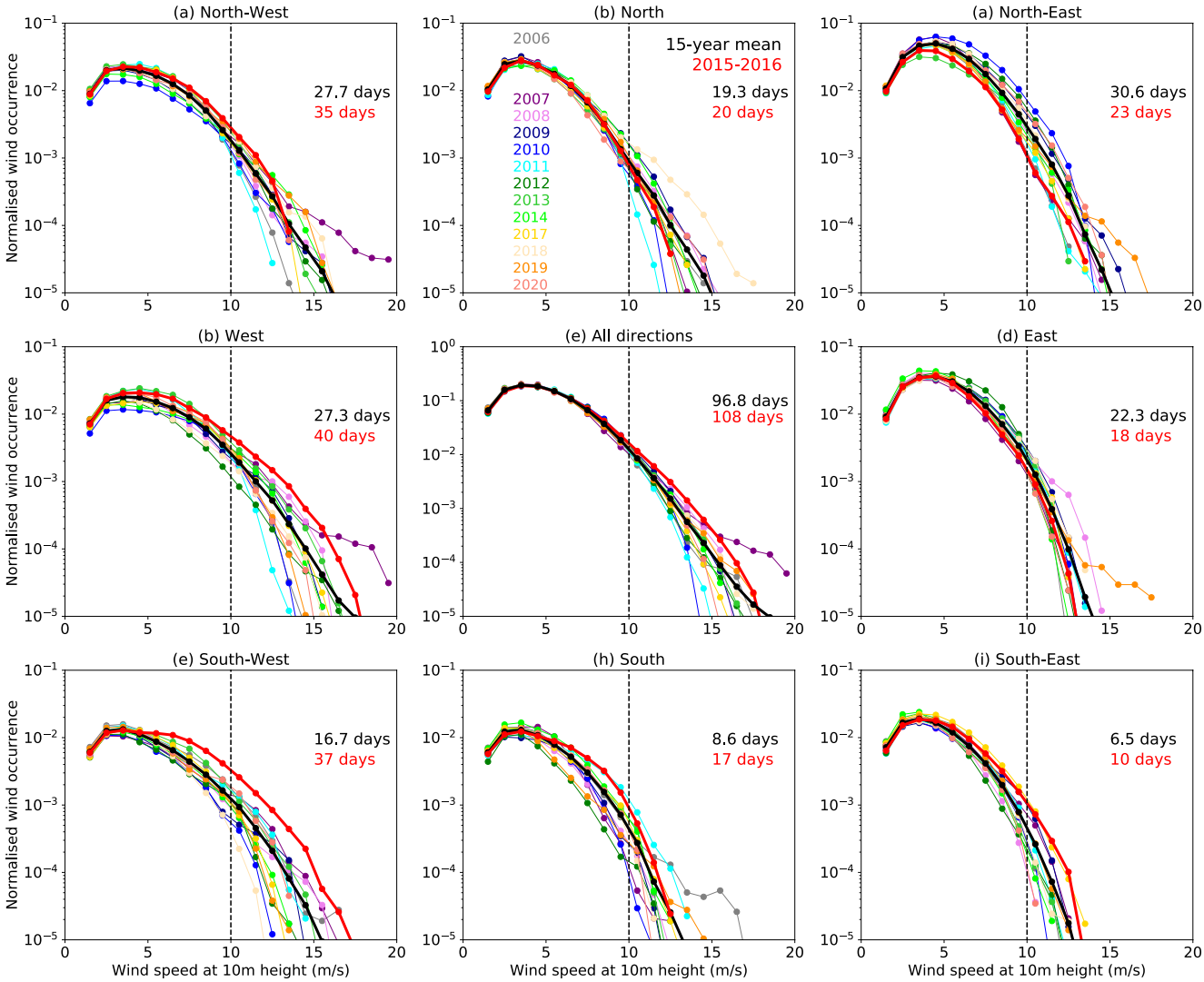

Figure 6. Yearly ERA5 surface wind distributions (at 10 m height) over the Aralkum for the eight directions around its basin, as labeled, between 2006 and 2020 (excluding the calendar years of 2015 and 2016). The red and black lines indicate the one-year period from April 2015 to March 2016 and the 15-year mean, respectively. The directions here refer to the directions from which the wind is coming, while the central panel represents the totality of all the directions. The number of days refers to the number of days on which the wind speeds exceed 10 m s^{-1} (to denote occasions with a particularly high potential for strong dust emissions) somewhere in the Aralkum at some point during the day. Each sector is 45° of arc.

also standing out as a wet month. Markedly below-average was the snow cover, not exceeding a monthly average of 10% anytime during the DUBLT year. Considering these two parameters together with their implications for dust emission, we may infer that summer and early autumn 2015 would have had a relatively high potential for dust emission (i.e., particularly dry). On the other hand, April, May, and November 2015 may have seen some extra suppression of dust emission due to above-average precipitation. The same could also be said of December 2015 and March 2016, however the above-average precipitation could be mitigated to some degree by the below-average snow cover: as will be discussed in Section 4.2, these two months saw some of the most substantial dust events simulated during the DUBLT year, implying that in the simulations the snow effect may have outweighed the precipitation effect at least for these months.

Returning to the specific DUBLT simulation year, during the winter the meteorological situation was characterized by an Arctic warming event in December 2015 (Moore, 2016). This had consequences for severe winter weather in North America (Cohen et al., 2018) and may have contributed to shifting weather patterns over Eurasia (He et al., 2020), an anomaly which may be associated with the wind patterns over the Aralkum shown in Figure 6. The increasing frequency of such Arctic warming events (Graham et al., 2017; Overland et al., 2021),

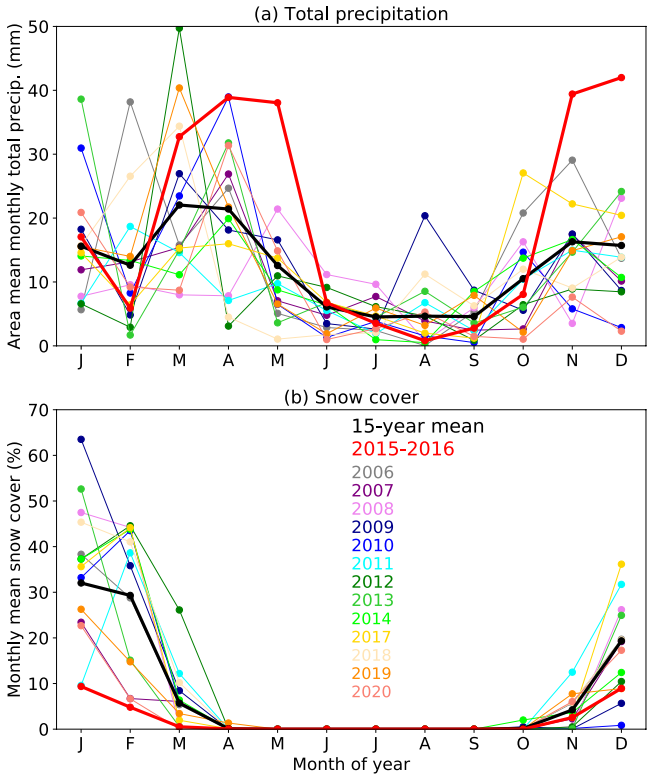

Figure 7. Similar to Figure 6, but as a yearly cycle for ERA5 monthly total precipitations and snow covers averaged over the Aralkum between 2006 and 2020, per year. The red and black lines indicate the one-year period from April 2015 to March 2016 and the 15-year mean, respectively.

associated with global warming, will therefore have an impact on the characteristic dust emission patterns of the Aralkum and of the wider Central Asian region. While the year of the DUBLT simulation that we present here in this paper is of necessity a 1-year case study, that cannot represent all of the possible dust emission patterns that the Aralkum may produce, the simulated winter of 2015–2016 may be indicative of characteristic Central Asian dust patterns which will become more prevalent in future years.

3.2. Patterns of Central Asian and Aralkum Dust Emissions

The first stage of the dust atmospheric life-cycle is dust emission: simulated seasonal dust emissions from the past and present DUBLT scenarios are mapped in Figure 8 and quantified on the monthly timescale in Figure 9, highlighting the extended dust source region of the Central Asian deserts of the Aralkum, the Karakum, and the Kyzylkum, to the north and east of the domain. The Aralkum and the Karakum are particularly active in spring, a feature also noted by Mohammadpour et al. (2022). In comparison with the Central Asian deserts the deserts in Iran and Afghanistan provide more discrete dust sources, particularly active in summer along the border between the two countries. The Sistan Basin in particular has its peak in emissions from July to August, tapering off in September down to a relatively low level during the autumn to the spring. Meanwhile to the far south-west the Iraqi deserts are simulated to produce their most substantial dust emissions in spring and summer, a well-known feature that has been previously noted by, for example, Notaro et al. (2015), Yu et al. (2016), and Banks et al. (2017).

Considering the differences between the past and the present scenarios, the total dust emission over the Central Asian domain for the past scenario is 180.3 Tg, while for the present scenario there is a 7 Tg increase to 187.3 Tg. To set these numbers in context, previous dust model intercomparison studies give a wide spread of global dust emission estimates between 735 and 8,186 Tg year^{-1} (Wu et al., 2020), while for North Africa and the Middle East dust emission estimates range from 400 to 2,200 Tg year^{-1} and 26 to 526 Tg year^{-1} (Huneeus et al., 2011). For the Aralkum, Xi and Sokolik (2016b) estimated emissions between 0.4 and 11.4 Tg year^{-1} depending on emission parameterization. Within the DUBLT scenarios the Aralkum is a major contributor to the increase over the Central Asian domain, the emission from its region is 14.3 Tg in the past and 27.1 Tg in the present, a near-doubling in its overall emissions and providing an extra ~7% to the regional Central Asian emissions. This is the outcome of the 25,000 km^2 expansion in the land area of the box, from a past land area of 103,000 km^2, which is also indicative of the high erodibility (short z_0, silty loam soils) of the assumed soil properties of the new Aralkum. It is obvious that the emissions from around the Aral Sea would have been even smaller in the decades prior to the "past" scenario, before the mid-1980s. Meanwhile on the overall regional scale the drying of the Hamoun Lake in the Sistan Basin is simulated to be relatively trivial, increasing from 14.5 Tg in the past to 14.8 Tg in the present, indicative of the relatively small size of this lakebed. Conversely, the inundation of the Garabogazköl Basin is reflected in the past emissions of 17.6 Tg, reduced to 11.7 Tg for the region in the present. At 5.9 Tg the simulated emissions from the 1980s lakebed of the Garabogazköl Basin are not inconsiderable, and as a consequence of their assumed silty loam soil properties they are comparable to the new emissions of 12.8 Tg produced over the larger area of the lakebed of the new Aralkum.

It is possible that the simulated present Aralkum emissions should be considered to be within the upper range of possible estimates, given the assumed snow coverage and soil properties. In particular, the central areas of the Aralkum are simulated to emit the most dust but are also where the potentially less-deflatable Solonchak soils are located. Meanwhile MODIS snow retrievals are very sparse over the basin of the former Aral Sea, with retrievals only ever present in 133 of the 201 grid cells within the Aralkum box (i.e., around the Aral Sea basin): scaling the snow coverage from the Aralkum box to include also the Aral Sea basin, we estimate that the simulated winter emissions of 7.9 Tg may need to be scaled downwards to 6.8 Tg, a modest decrease. The yearly total would then

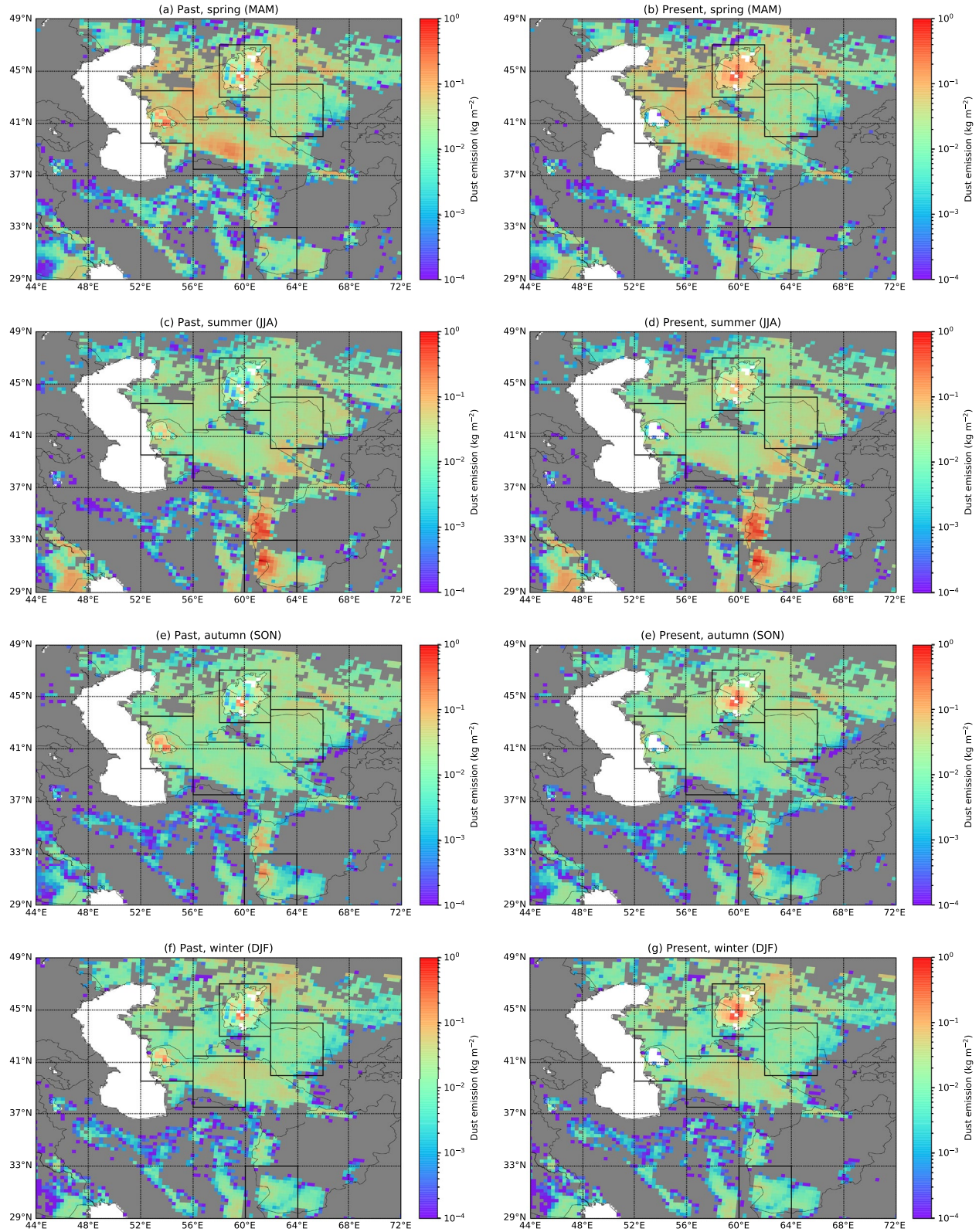

Figure 8. Maps of seasonal total dust emissions produced by the past (left column) and present (right column) DUBLT scenarios. Of the present yearly emissions for the Central Asian region, 32.4% occur in spring, 31.8% in summer, 17.4% in autumn, and 18.3% in winter. The total past emission for the year is 180.3 Tg, while for the present it is 187.3 Tg; meanwhile in the Aralkum box (marked in black) the past and present emissions are 14.3 and 27.1 Tg.

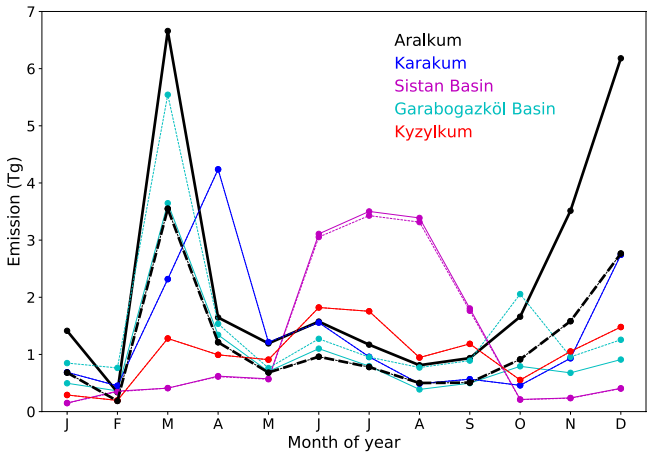

Figure 9. Monthly dust emissions produced by the present DUBLT scenario for five similarly sized regions within the Central Asian domain. The "Aralkum" region is here bound by 43°–47°N, 58°–62°E, the "Karakum" is within 37.5°–41.5°N, 56°–60°E, the "Sistan Basin" is within 29°–33°N, 60°–64°E, the "Garabogazköl Basin" is within 39.5°–43.5°N, 52°–56°E, and the "Kyzylkum" is within 40°–44°N, 62°–66°E. Dashed lines indicate the past emissions, the solid lines the present: these overlap for the Karakum and the Kyzylkum boxes, both of which are old deserts where there is no appreciable difference in surface water coverage between the two epochs.

be 25.6 rather than 27.1 Tg. The bulk of the Aralkum's winter emissions (Figure 9a) occur in December, shortly prior to the arrival of the most widespread snow cover periods in January and February.

With respect to the soil, spatially the most concentrated simulated dust emissions within the Aralkum are over the south-central parts of the basin, over those relatively newly-dried grid cells which used the soil properties based on those measured by Argaman et al. (2006), soil properties which have a particularly high silt content and hence particularly high values of the sand-blasting efficiency α. Neighboring deserts such as the Karakum and Kyzylkum tend to have a higher clay content than the central Aralkum, and hence lower values of α. Newly-dried, these central Aralkum grid cells also have higher surface water fractions compared to older and drier Aralkum grid cells to the east, where SoilGrids data are available. Between the three major desert regions in Central Asia, the Aralkum is simulated to emit 27.1 Tg, the Karakum 16.6 Tg, and the Kyzylkum 12.5 Tg. A caveat here is that it is obvious that the square boxes do not correspond exactly to the boundaries of these deserts, however these do correspond approximately to the boundaries and with approximately equal areas they make for a fair comparison in terms of the dust emission intensities. Based on site measurements, Opp et al. (2019) reported average dust depositions over the Aralkum to be 152 kg ha^{-1} month^{-1}, over the Karakum to be 125 kg ha^{-1} month^{-1}, and over the Kyzylkum to be 248 kg ha^{-1} month^{-1}: with another caveat that emissions and depositions are not the same concept, they are nonetheless closely correlated to each other over the desert source regions, and these measurements therefore imply that the DUBLT simulations may produce too much dust from the Aralkum with respect to the Kyzylkum. This suggests that it may be sensible to regard the simulated emissions from the Aralkum as an upper estimate, or conversely, that the emissions from the older deserts are under-represented by the DUBLT scenario.

Focusing on the dust emission behavior that these meteorological conditions give rise to in the Aralkum, Figure 10 characterizes the present-era dust emission from the Aralkum region in relation to the average wind speed and direction at emission, by season, along with the frequency of these wind speeds and directions. The patterns, although not the intensities, are broadly similar for the past-era dust emissions, and hence for brevity they are not shown here. The most common direction from which winds arrive on the Aralkum is from the north-east quadrant (left column in Figure 10), in particular with average wind speeds between 3 and 5 m s^{-1}. During the course of the year 31.5% of the winds are from the east, 28.2% from the north, 25.2% from the west, and 15.1% from the south. The dominant north-easterly wind direction appears to be consistent with the findings of Semenov (2012), who compared surface dust observations with wind measurements from meteorological stations to infer that often dust emissions from the Aralkum are driven by north-easterly winds and hence are initially transported south-westwards. However in the DUBLT simulation year these common north-easterly wind speeds are not simulated to drive the bulk of the emissions (middle column in Figure 10), which are instead driven by rarer stronger winds which may come from various directions. In the peak spring and winter months the emissions appear to be driven mostly by westerly winds, a feature also considered by Ge et al. (2016) who used HYSPLIT (Hybrid Single-Particle Lagrangian Integrated Trajectory) simulations to highlight the potential for north-eastwards long-range dust transport from the Aralkum in these seasons. During the year, 14.5 Tg of dust is simulated to be emitted by westerly winds, compared to 4.8 Tg by northerly, 4.2 Tg by easterly, and 3.5 Tg by southerly winds. It is therefore to be expected that Aralkum dust events during the DUBLT year will primarily head eastwards, an apparent contradiction with the patterns observed for other years by Semenov (2012), Issanova et al. (2015), and other authors. These patterns are however entirely consistent with the ERA5 wind patterns displayed in Figure 6, which showed how the DUBLT year was marked by an above-average frequency of strong westerly winds.

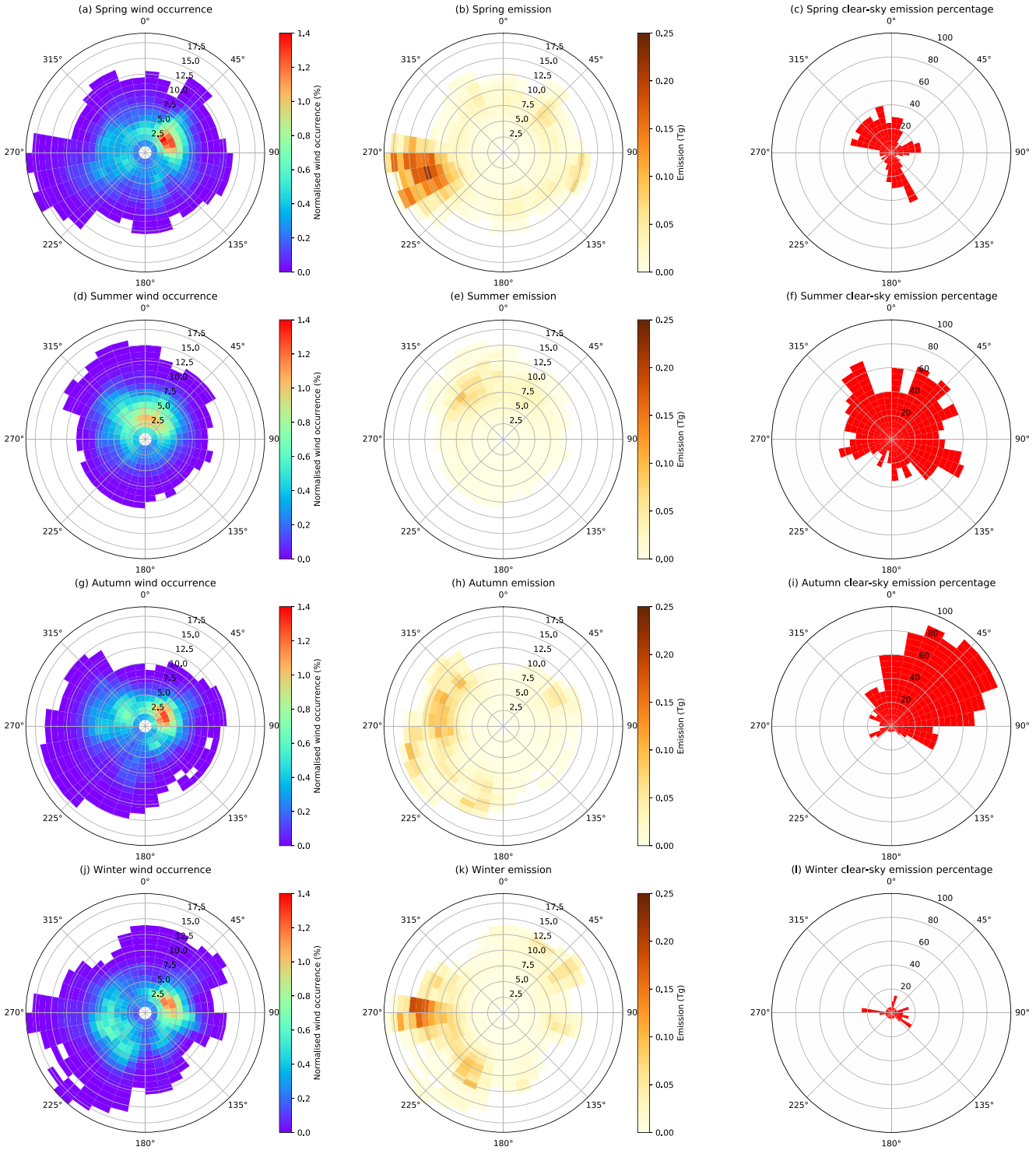

Figure 10. Polar heatmaps of the normalized frequency of occurrence (%) of surface wind speeds and directions (left column) from which they flow over the Aralkum region, the total emissions (Tg) produced in the present DUBLT scenario by these wind speeds and directions (middle column), and (right column) the percentages of the total emissions simulated under clear-sky conditions with a cloud cover of <5%, marked in red. Winds and cloud cover are the simulated output from COSMO. In the right column, white indicates the percentages of emissions produced when the cloud cover is >5%. (a–c) spring (MAM), (d–f) summer (JJA), (g–i) autumn (SON), (j–l) winter (DJF). The upper threshold of wind speeds depicted is 20 m s^{-1}. In the left and middle columns, white indicates no occurrence of a wind speed from the given direction. Note that emission from westerly winds (e.g., panel (b)) implies emission in the eastwards direction.

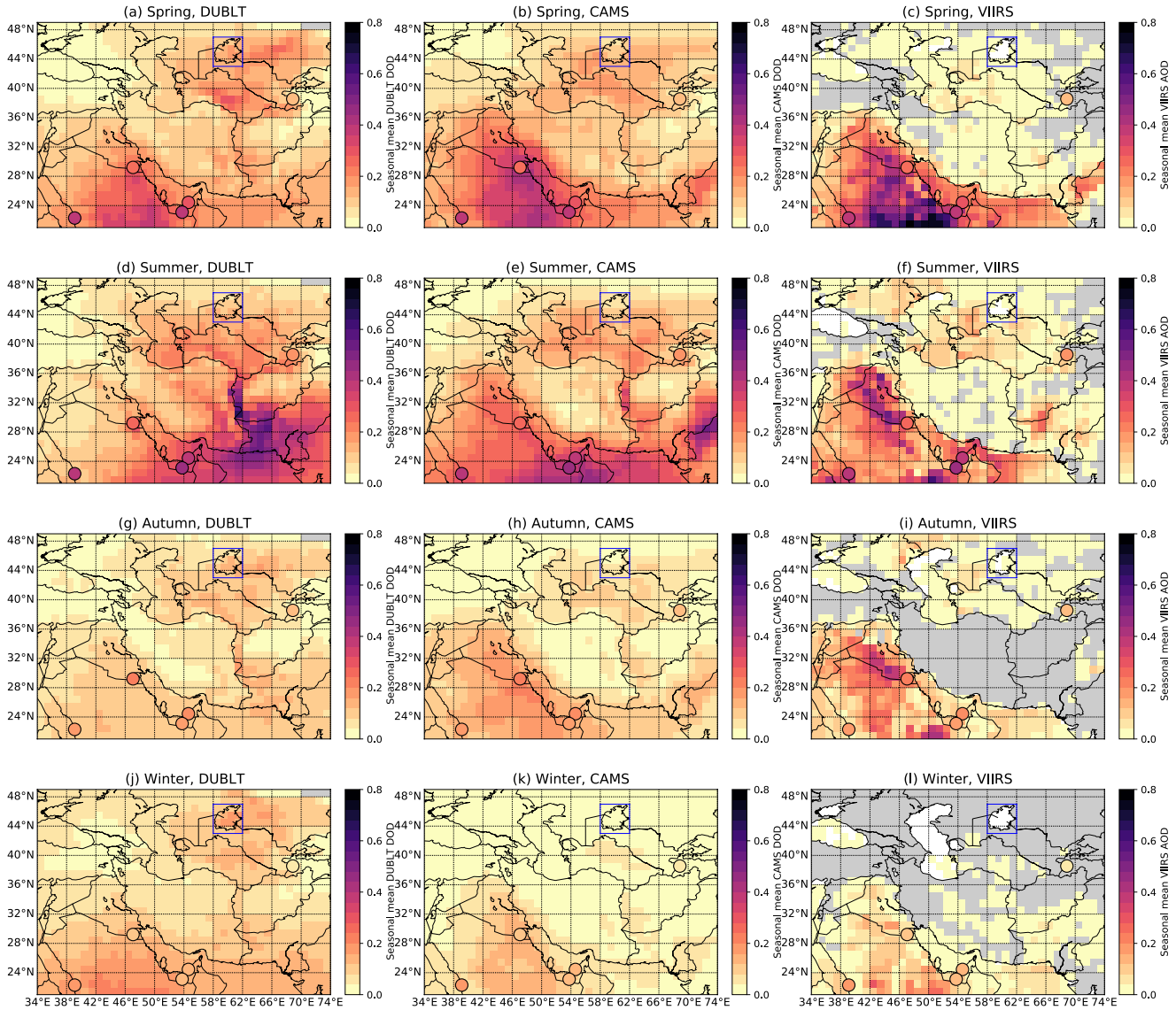

Figure 11. Seasonal mean dust aerosol optical depths (DODs) as simulated by the DUBLT scenario (left column) and the CAMS reanalysis (middle column) at 09:00 UTC, and AODs as retrieved by Visible Infrared Imaging Radiometer Suite (VIIRS) (right column). 09:00 UTC is approximately the local time of the VIIRS overpasses of the Central Asian region. Seasonal mean AERONET coarse-mode AODs (where available) for the sites of Dushanbe (Tajikistan), KAUST Campus (Saudi Arabia), the Masdar Institute (UAE), Mezaira (UAE), and Shagaya Park (Kuwait), are included as overlaid circles on each map, with the same color bar. The Central Asian domain is here expanded in order to include the AERONET sites on the Arabian Peninsula. The blue square identifies the Aralkum. Note that the VIIRS data subset is only from successful retrievals, while the DUBLT and CAMS averages are computed from all 09:00 UTC timeslots.

4. Dust Transport Over Central Asia

Progressing to the next stage in the dust life-cycle, the left column of Figure 11 displays the seasonal mean DODs simulated by the DUBLT scenario over Central Asia and including the Arabian Peninsula. Summer is identified as a particularly significant period for dust presence over Afghanistan, Pakistan, and south-eastern Iran, due in large part to the Levar wind's substantial effects on the Sistan Basin and its neighboring deserts. Over Iraq and the Arabian Peninsula the peak months appear to be in spring, with the center of the average dust presence shifting eastwards across the Peninsula going into summer. Meanwhile over the Aralkum spring appears to be the peak period of dust presence in the region, manifesting also a clear downwind pattern of dust heading eastwards predominantly over Kazakhstan.

4.1. AOD Comparisons With AERONET and VIIRS Retrievals, and CAMS Simulations

Validation of the DUBLT simulations over the Central Asian region is heavily constrained by the lack of ground-based aerosol measurement sites in the region. Sun-photometer measurements from AERONET sites (Aerosol Robotic Network: Holben et al., 1998) are traditionally used as a primary source of validation measurements both for aerosol models and for satellite aerosol retrievals, as the most direct form of columnar aerosol measurements, however within the DUBLT domain the AERONET site at Dushanbe is the closest AERONET site to the Aralkum (~1,025 km from the center of the Aralkum). Five other AERONET sites relevant to dust within and close to the Central Asian domain may also be considered for the 2015–2016 period, with one in Pakistan and four on the Arabian Peninsula, but which are sufficiently far away that dust from the Aralkum and its nearby deserts does not provide any meaningful contribution to their aerosol conditions. Moreover, the site in Pakistan (Karachi) is dominated by aerosols other than dust. Satellite aerosol retrievals would appear to be the main available source of validation data over Central Asia, despite frequent cloud cover obscuring the Aralkum. For this purpose we consider aerosol optical depth (AOD) retrievals from the Visible Infrared Imaging Radiometer Suite (VIIRS) onboard NASA's Suomi NPP satellite, as described by Sayer et al. (2018), Hsu et al. (2019), and Sayer et al. (2019). Daily Level 3 AOD data have been chosen, from the AERDB_D3_VIIRS_SNPP data set, at a resolution of $1 \times 1°$. However, given the known challenges for satellite aerosol retrievals in the Central Asian region posed by clouds, it is instructive also to consider comparisons with the CAMS EAC4 (ECMWF Atmospheric Composition Reanalysis 4) reanalysis data set of aerosol composition (Inness et al., 2019), to provide state-of-the-art global model estimates of dust aerosol distribution. The aerosol component of the CAMS model is assimilated with MODIS satellite AOD retrievals (Levy et al., 2018), which only uses "Deep Blue" dust aerosol retrievals where "Dark Target" aerosol retrievals are not available. It is relevant to note that it is the total AOD from MODIS that is assimilated (not subdivided by aerosol type) and that therefore the aerosol species' contributions to the aerosol loading must be computed within the model, contributing an extra source of uncertainty within the CAMS reanalysis. In the context of assimilated MODIS retrievals, the usage of VIIRS aerosol retrievals for comparison with DUBLT and CAMS, rather than MODIS retrievals, provides an additional source of independent data. All three data sets are interpolated onto a common $1 \times 1°$ grid, with VIIRS grid cells only chosen when the aerosol type identified is either "Dust" or "Mixed", with an Ångström coefficient of less than 0.6 (to mitigate against the inclusion of aerosols other than dust, e.g., Dubovik et al. (2002)), and with at least 100 retrievals within each grid cell (out of ~400–600 pixels).

The middle and right columns of Figure 11 map the seasonal mean DODs simulated by CAMS and AODs retrieved by VIIRS, along with the measurements made at the five AERONET sites. Of the three DUBLT simulation scenarios, only the present DUBLT scenario is intended to portray the present-era dust distributions. All three sets of measurements and simulations highlight the predominance of dust over the Arabian Peninsula in spring, although VIIRS retrieves more intense dust loadings than the DUBLT and CAMS simulations depict. There is also general agreement between the retrievals and simulations as to the seasonal peak in dust loading over southern Afghanistan/western Pakistan in summer, the main disagreements being the exact locations and intensities. VIIRS does not retrieve aerosol over the inner Aralkum, indicating a typical difficulty that satellite aerosol retrievals have in this region of shifting surface water coverage (e.g., Carroll et al., 2017). There is also a paucity of VIIRS retrievals in the northern half of the domain during winter, a consequence of frequent cloud cover during these months. Retrievals are also made more difficult in winter by snow cover. In contrast, both DUBLT and CAMS are able to simulate dust over the Aralkum and under cloudy conditions, and over snow. Both DUBLT and CAMS highlight the presence of dust over Turkmenistan's Karakum Desert, predominantly during spring and summer, whereas VIIRS only appears to retrieve appreciable amounts of dust in the Central Asian deserts in summer. The peaks in model DODs in spring and summer are however consistent with two previous Central Asian studies that made use of MODIS data: Rupakheti et al. (2019) analyzed Aqua-MODIS retrievals to highlight the importance of these seasons within an aerosol climatology for the Central Asian countries, identifying mean AODs of 0.20 ± 0.10 over Turkmenistan, with spring and to a slightly lesser extent summer being the particularly dusty seasons for this country. Meanwhile Nobakht et al. (2021) used MODIS imagery over a 10-year period to identify dust emission point sources, and also found a primary peak in dust activity over the Karakum in summer and a secondary peak in spring, a finding which is not inconsistent with either of the models or with VIIRS.

Statistical comparisons with AERONET over the five sites (Table 1) show rather closer agreement between VIIRS and AERONET than between the models and AERONET, an unsurprising outcome given that AERONET

Table 1
VIIRS, DUBLT, and CAMS AOD Statistical Comparisons With AERONET (AER), From Co-Located Data Where Both VIIRS and AERONET Make Successful AOD Retrievals

Site	VIIRS/AER	DUBLT/AER	CAMS/AER
Dushanbe			
Tajikistan			
R^2	0.77	0.68	−0.33
Bias	−0.03	−0.06	−0.21
RMSD	0.07	0.18	0.25
RMSD/$\overline{\text{AOD}}$	0.19	0.50	0.69
KAUST Campus			
Saudi Arabia			
R^2	0.94	0.42	0.83
Bias	+0.24	−0.29	−0.17
RMSD	0.27	0.41	0.25
RMSD/$\overline{\text{AOD}}$	0.58	0.88	0.55
Masdar Institute			
UAE			
R^2	0.92	0.64	0.66
Bias	+0.20	−0.10	−0.06
RMSD	0.21	0.17	0.14
RMSD/$\overline{\text{AOD}}$	0.62	0.49	0.42
Mezaira			
UAE			
R^2	0.94	0.56	0.84
Bias	+0.38	−0.12	−0.06
RMSD	0.42	0.23	0.14
RMSD/$\overline{\text{AOD}}$	1.30	0.71	0.44
Shagaya Park			
Kuwait			
R^2	0.80	0.32	0.72
Bias	+0.29	−0.08	−0.03
RMSD	0.33	0.19	0.13
RMSD/$\overline{\text{AOD}}$	1.53	0.88	0.58

Note. R^2 denotes the correlation, RMSD denotes the root-mean-square difference, and $\overline{\text{AOD}}$ is the subset mean coarse-mode AERONET AOD, which for the five sites (with numbers of points in parentheses) are: 0.37 in Dushanbe (6), 0.47 at KAUST Campus (91), 0.34 at the Masdar Institute (15), 0.32 in Mezaira (65), and 0.22 in Shagaya Park (47).

and VIIRS are both within the observation space while CAMS and DUBLT are both simulations. CAMS generally displays closer agreement over the Arabian Peninsula compared to the DUBLT scenario, with notably higher correlations, less negative biases, and smaller RMSDs, indicating the relative weakness of the DUBLT model performance in this region. As an assimilation model, CAMS has an advantage over relatively cloud-free regions that the MODIS AODs can be readily integrated into the model, an advantage that a free-running model such as DUBLT does not have. Meanwhile CAMS exhibits weaker statistical comparisons over Dushanbe.

What all these comparisons show is that the DUBLT simulation typically underestimates how much dust there is in the atmosphere; CAMS does this too, but to a lesser extent. DUBLT is particularly low-biased over the Arabian Peninsula, while over Central Asia (the Aralkum and Kazakhstan south to Pakistan) the DUBLT scenario simulates more dust, values that are on average closer to those measured by AERONET and retrieved by VIIRS. The Sistan Basin and the Pakistan/Afghanistan/Iran tri-border area is a region that is a particular hotspot for DUBLT DODs in summer, a consequence of favorable soil properties in the model and reliably strong simulated winds during this season.

4.2. Aralkum Dust Emission, Cloud Cover, and Satellite Remote Sensing Observations

Observing the formation of Aralkum dust storms would appear to be complicated by the cloud cover associated with the driving wind conditions. Of the 27.1 Tg of the Aralkum's simulated emissions for the year, 18.5 Tg (i.e., 68%) are emitted under cloudy skies with a cloud coverage of >95%. In contrast, only 4.5 Tg are emitted under clear skies with a cloud coverage of <5%. Thus the dominant portion of these dust emissions cannot be corroborated by satellite observations and measurements, constrained as they are in their aerosol retrievals by the requirement for clear skies. This highlights what is simultaneously an advantage and a disadvantage of the modeling approach: on the one hand we may be able to use it to infer what may be happening which cannot be observed, while on the other hand there may be very few quantitative aerosol retrievals available to validate it. Moreover, the COSMO cloud simulations over the Aralkum are not uniquely cloudy amongst meteorological models: over the year the average Aralkum area mean cloud cover is simulated by COSMO to be 50.7%, while the equivalent ERA5 reanalysis cloud cover is 45.9%, with the two data sets correlated to a value of 0.82 (built on a time-series of area-averaged cloud covers).

Returning to Figure 10 from Section 3.2, the right column displays the percentages of the Aralkum's dust emissions produced under clear-sky conditions with cloud cover <5% (red), and which may be observable by satellite and by ground-based remote sensing instruments. The remaining percentages of emissions produced under cloudier skies are indicated in white. The percentages of the overall emissions that occur under the clear-sky conditions are 11% in the spring (1.0 Tg from a seasonal total of 9.3 Tg of emission), 48% in the summer (1.7 Tg from 3.5 Tg), 20% in the autumn (1.2 Tg from 6.1 Tg), and just 6% in the winter (0.4 Tg from 7.9 Tg), with summer standing out as the season with the least emissions in absolute terms occurring under cloudy skies and also the most emissions under clear skies, primarily driven by northerly and easterly winds. It is therefore the case that very little of spring's substantial westerly wind-driven dust emissions occur under clear skies. This implies the risk that observational studies of Aralkum dust may be heavily biased by the conditions that permit dust to be observed, and that major dust events may be

Table 2
Directional Dust Emissions (Tg) From the Aralkum During the Course of the DUBLT Simulation Year, for All-Sky and Clear-Sky (Cloud Cover <5%) Conditions

Direction	All-sky	Clear-sky
Northerly	4.8	1.7
Westerly	14.5	1.5
Southerly	3.5	0.2
Easterly	4.2	1.1
Total	27.1	4.5

missed: satellite instruments are likely to detect the most dust in the summer of the DUBLT year, even if the simulations suggest that this is not necessarily the season that produces the most dust (i.e., spring). As shown in Table 2, in contrast to the all-sky dust emissions where westerly winds drive over half of the yearly dust emissions, under clear skies northerly winds produce the most dust, with 1.5 Tg driven by westerlies and 1.7 Tg by northerlies. During this simulated year satellite observational studies would therefore reach very different conclusions as to the dominant patterns of Aralkum dust transport. This is not to say that satellite studies cannot observe similar seasonal patterns: as noted previously, Nobakht et al. (2021) used multi-year MODIS imagery and found a typical spring peak in Aralkum dust emissions followed by a secondary peak in summer. These observed peaks show some comparability with the DUBLT simulations, in which spring and summer are the peak of the all-sky and clear-sky emissions, respectively.

What does this mean for the possibility of observing specific Aralkum dust events? Figure 12 provides a visual description of three dust events that occurred during the DUBLT year, as simulated by the DUBLT scenario and as observed by true-color Aqua-MODIS imagery. These are three significant and characteristic events which relate the seasonal meteorology (as previously described) in summer, winter, and spring to their consequences for dust activity. For context, ranking the days with respect to their contribution to the yearly emissions from the Aralkum, 13 June 2015 was the day that emitted the twelfth highest amount of dust (0.41 Tg), 18th December emitted the third highest (1.24 Tg), and 17 March 2016 emitted the sixth highest (0.86 Tg). During the DUBLT simulation year, the clearest Aralkum dust events observable in the MODIS imagery are directed toward the south-east. As an example of this, 13th June (panels (a) and (b)) is an important contributor to the summertime south-eastwards transport of Aralkum dust, clearly visible in the MODIS image in two main bands from the southern basin of the Aralkum, to either side of what remains of the eastern lobe of the South Aral Sea. The DUBLT scenario also represents this event, although it seems that there is a discrepancy in the timings, with the simulated dust storm appearing to occur ∼6 hr later than the observed event. A similar event is observed by MODIS and simulated by DUBLT on 17th July.

The picture becomes murkier going into winter and early spring. The December and March events (panels (c–f)) display two occasions when the Aralkum's dust storms were driven by westerly winds, and highlight the difficulty of observing these events. The day prior to the March event, 16 March 2016, was the day on which the Aralkum emitted the most dust in a single day, 2.54 Tg, however this day was largely shrouded by cloud, both as observed by MODIS and as simulated by COSMO-MUSCAT (91.6% as a daily average across the Aralkum box). 16th March was the major example of a simulated Aralkum dust storm driven by westerly winds. However the same weather system lasted into the next day and again emitted dust in the eastwards direction, but with only 69.8% cloud cover there was more possibility to observe this event (panel (f)), visible as a streak heading directly eastwards from the Aralkum. Finally, the eastwards dust streak on 18th December (panels (c–d)) is also made difficult to observe due to nearby (but not co-located) cloud cover, although here an added complication is provided by the widespread thin layer of snow over which the dust is transported. The DUBLT scenario simulates 1.24 Tg of emission on this day, out of the 7.93 Tg that it simulates for the whole winter. It is apparent that eastwards dust events were characteristic of the winter of 2015–2016.

4.3. Sphere of Influence of Aralkum Dust

The influence of the Aralkum on dust loading over its neighboring regions is broken down in Figure 13, considering its transport in eight directions, overlaying the mean DODs from the DUBLT_PAST and the DUBLT_ARAL scenarios alongside those from the DUBLT scenario in order to isolate the significance of dust from the Aralkum within the region. In every direction bar the southern direction, with respect to distance the central 100 km of the Aralkum has the highest DOD in the DUBLT scenario, indicative of the Aralkum's status as one of the major dust sources within the Central Asian region. In the southern sector there is a higher peak in DOD ∼700 km south of the Aralkum in the Karakum Desert, just to the north of Ashgabat. Similarly to the south-east there is another peak at ∼600 km, in the Kyzylkum Desert. Meanwhile to the south-west there is the clear signature of

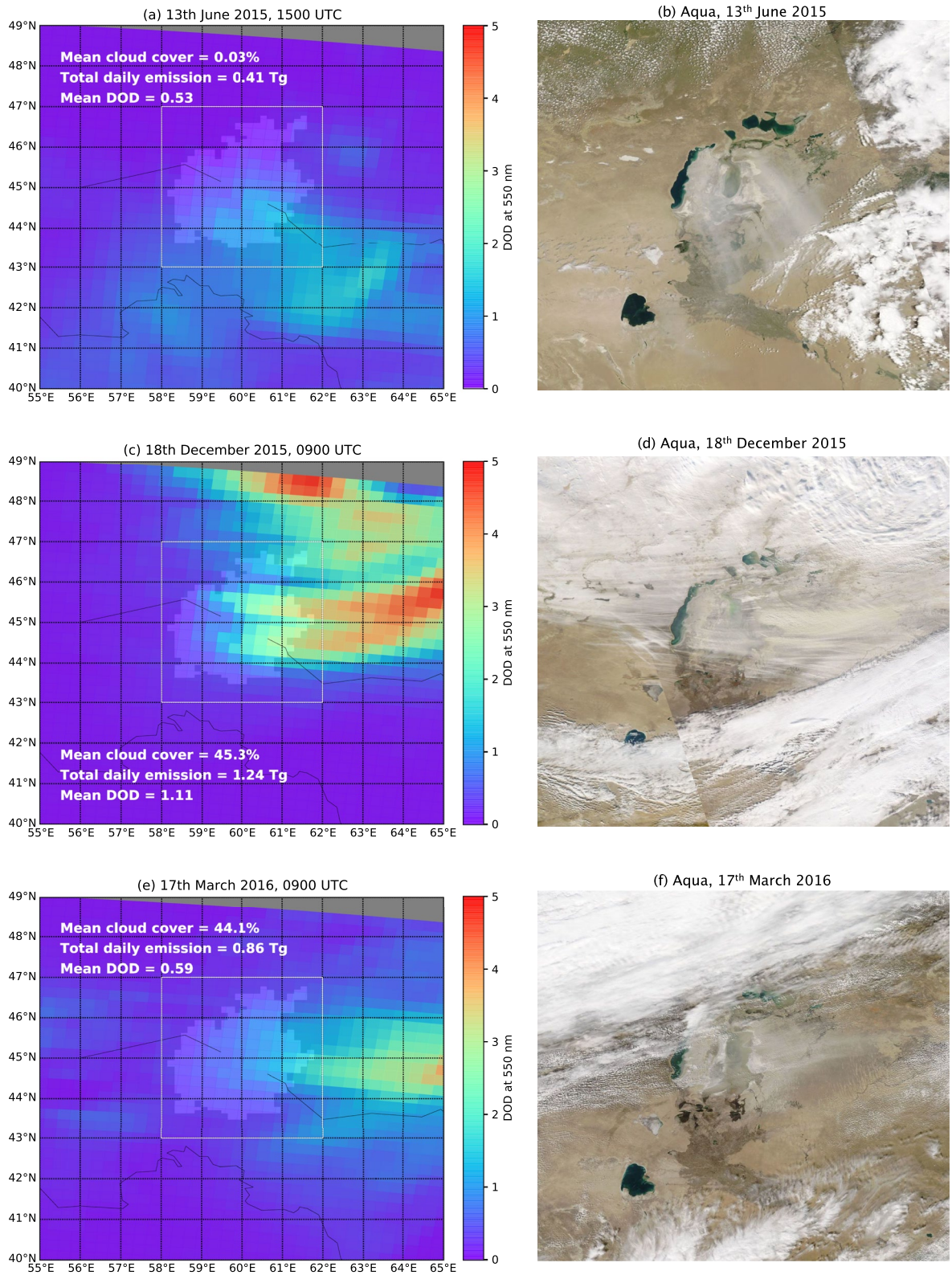

Figure 12. Instantaneous DUBLT dust aerosol optical depth (DOD) (left column) over the Aralkum for three sample dust events, and (right column) near-simultaneous Aqua-MODIS true color images. The DODs and the MODIS images have the same spatial extent of 40°–49°N, 55°–65°E. The instantaneous mean cloud covers and DODs, and daily emissions, refer to the spatial region within the white Aralkum box. Aqua crosses the equator at ~1,330 local time, approximately 09:30 UTC over the Aralkum. MODIS images obtained 20 January 2022 from https://worldview.earthdata.nasa.gov.

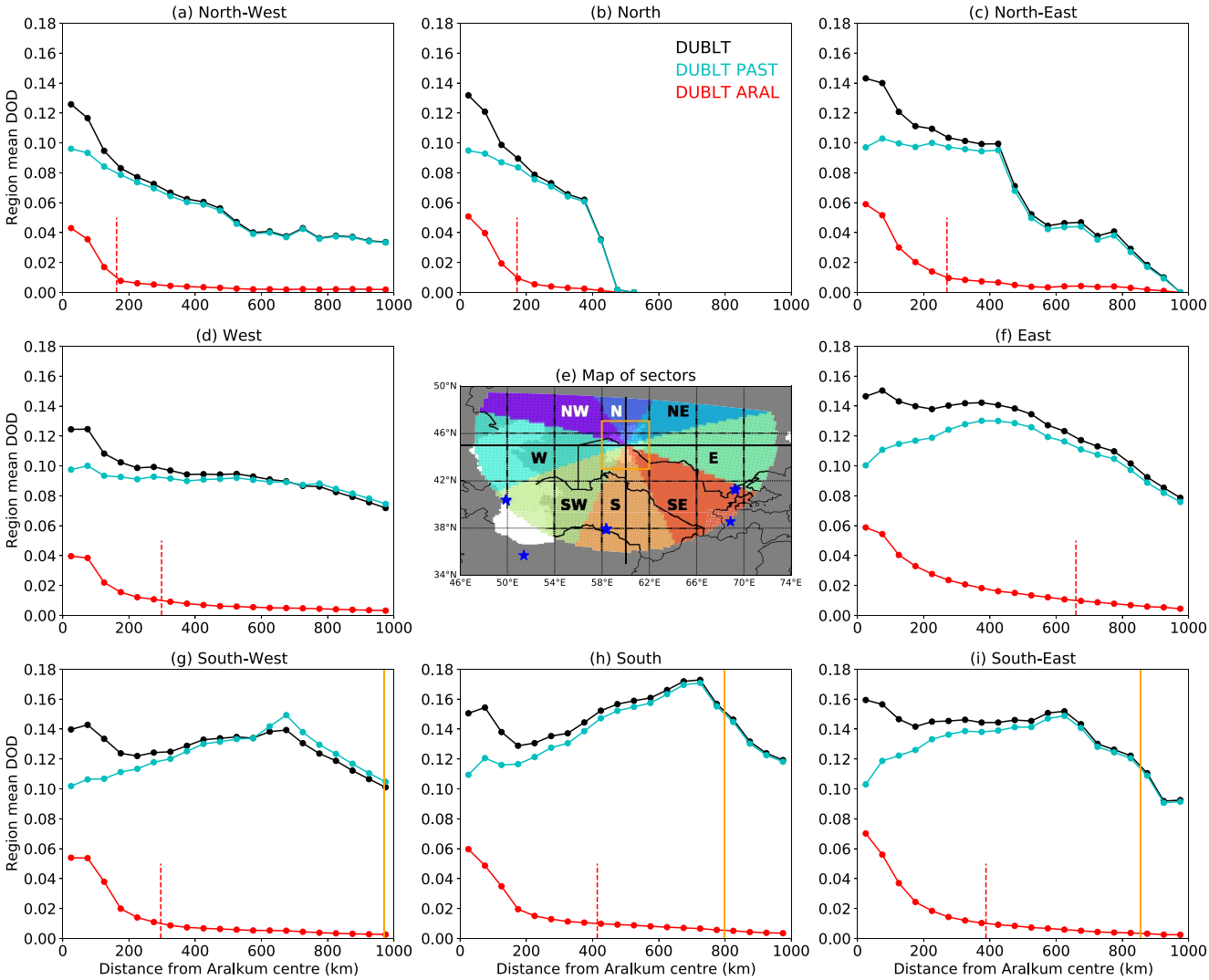

Figure 13. Yearly mean DODs as a function of distance from the center of the Aralkum (for simplicity here considered to be 45°N, 60°E), for the eight directions in which dust is transported outwards from its basin, as labeled. All three scenarios are included, in order to highlight the contribution of newer dust sources within the Aralkum to the regional dust loadings. Each spatial bin is 50 km across, and 45° of arc. The orange lines in panels (g–i) indicate the locations of the cities of Baku, Ashgabat and Tashkent, respectively, with white stars marking some relevant cities in panel (e). The regional mean DUBLT and DUBLT_ARAL DODs are 0.101 and 0.003 for Baku, 0.157 and 0.006 for Ashgabat, and 0.110 and 0.003 for Tashkent. The red dashed vertical lines indicate the distances at which the mean DUBLT_ARAL DODs sink below 0.01. Note that the distances in the northern directions are truncated by the edge of the domain.

the Garabogazköl Basin at ~650 km, where the mean DUBLT_PAST DOD has a value of 0.15, compared to the mean DUBLT DOD of 0.14.

Within the innermost 100 km around the Aralkum center the mean DUBLT_ARAL DODs range from 0.04 to 0.07, compared to mean DUBLT DODs in the same area ranging from 0.12 to 0.16, indicating that on the yearly average slightly under half of the dust loading over the Aralkum originates from the Aralkum itself. It is obvious that at longer distances from the Aralkum the contribution of the Aralkum's dust tails off, such that on the yearly average its contribution to the dust loadings over the cities marked in Figure 13 is negligible. In contrast, the Aralkum's instantaneous impact on these cities can occasionally be noticeable: during the year the maximum DUBLT and DUBLT_ARAL DODs are 2.99 and 0.17 over Ashgabat, 2.87 and 0.06 over Baku, 3.16 and 0.09 over Dushanbe, and 2.30 and 0.26 over Tashkent. Of the cities in the DUBLT scenario, Dushanbe appears to have received the most dust in one event, dust that originated from the Karakum in April 2015. As close neighbors to the deserts in their countries, Ashgabat and Tashkent appear to be the cities most frequently affected by dust, including also from the Aralkum, with DUBLT DODs >1 during 18 and 27 timeslots respectively, that is, during

the course of 54 and 81 hr during the year. Meanwhile Baku and Dushanbe are affected by such dust loadings during the course of 33 and 39 hr during the year.

What does all this imply for the likely consequences of the Aralkum's dust activity in the region? The major regional cities appear to be only very occasionally impacted by dust from the Aralkum, and those that are tend to be south- and south-eastwards from it. Settlements closer to the Aralkum are naturally more affected by it, from the red lines in Figure 13 (solid and dashed) we can estimate that dust produced by the Aralkum is particularly hazardous approximately within the innermost 200 km around the Aralkum centre, and out to even greater distances (400–600 km) to the south and east. The major population centres within this radius tend to be clustered along what remains of the ends of the Syr Darya and Amu Darya rivers, to the east in Kazakhstan and to the south in Uzbekistan, respectively. These would also be the settlements worst affected by the loss of water in these two rivers, indicative of how these settlements have been hit by a double disaster with respect to the destruction of the Aral Sea. Particularly badly affected by dust during the DUBLT simulation year would be the Kazakh settlements along the Syr Darya, noting that on the yearly average in the eastward sector there is still an appreciable amount of Aralkum dust out to a radius of ∼650 km, a situation which may be at its worst in winter and spring. For example, directly to the east of the Aralkum in the Kazakh town of Kazaly (also a site for deposition measurements, see Section 4.4), the simulated PM_{10} (particulate matter with a diameter <10 μm) values solely due to the Aralkum's dust exceed WHO air quality guidelines (World Health Organization, 2021) on 48 days during the year, with a yearly average of 36.8 μg m^{-3}. The WHO's guidelines provide a useful point of reference for acceptable air quality with respect to human health. The WHO's yearly mean threshold for PM_{10} is 15 μg m^{-3} and the daily mean threshold is 45 μg m^{-3}. Kazaly therefore greatly exceeds the yearly threshold due to Aralkum dust alone, which has severe consequences for human health given the contamination of Aralkum soils noted in Section 1.1 (Wiggs et al., 2003). Meanwhile the cities of Tashkent and Ashgabat exceed the daily threshold respectively on 2 and 3 days during the year from Aralkum dust, and Dushanbe not at all. The local Karakum and Kyzylkum are the major sources of dust pollution for these cities, exceeding the daily threshold on up to 145 days in Ashgabat in the present scenario.

4.4. Dust Deposition

Another consequence of the Aralkum's dust activity is its contribution to dust deposition in the region. The yearly dust dry and wet depositions are mapped for the three DUBLT scenarios in Figure 14, alongside the yearly mean DODs. Inevitably the deposition and DOD patterns are smoother and less discrete than the emission patterns in Figure 8, including sink patterns downwind of the source regions. Surrounded by barren land, the Aral Sea is simulated to have been a frequent sink of atmospheric dust including in the past, and has become a bigger sink in the present due to its own increasing role as a source. Note also the influence of the Garabogazköl Basin on the Caspian Sea, with a clear westwards deposition pattern noticeable in the past but not in the present: it is reasonable to speculate that the Garabogazköl Basin would have contributed to the mineral content of the central Caspian Sea during the 1980s. Panels (g) and (h) describe the specific DUBLT_ARAL deposition patterns, the longer deposition tails to the east compared to those to the west corroborating the DOD patterns displayed in panel (i). The wet deposition maps often display more heterogeneous patterns than the dry deposition maps, as a more discrete process.

As was discussed in Section 4.1, verifying the DUBLT simulation's estimates of Aralkum dust activity is problematic with remote sensing methods. Comparisons may also be possible, however, with dust deposition measurements carried out by various authors, for example, Groll et al. (2013) and Opp et al. (2017) who performed measurements at various sites in Kazakhstan, Uzbekistan, and Turkmenistan. As mentioned in Section 3.2, Opp et al. (2019) used measurements carried out between 2006 and 2012 over 23 sites in the three countries to calculate monthly average dust deposition aggregated among the sites in the Aralkum of 152 kg/ha, in the Karakum of 125 kg/ha, and in the Kyzylkum of 248 kg/ha, that is, 1,824, 1,500, and 2,976 kg/ha per year. These are rather more than simulated by DUBLT, which simulates yearly totals for 2015–2016 of 699 kg/ha averaged for the four sites in the Aralkum, 801 kg/ha for the sites in the Karakum, and 405 kg/ha for the sites in the Kyzylkum. Note that the measurements and the simulations occur during different years, with different wind patterns, so the comparison can only be indicative. Another part of the explanation for these differences in depositions may be relatively low emissions simulated by the DUBLT scenario, especially over the Kyzylkum and the Karakum but also perhaps over the Aralkum. Further, it may be that COSMO-MUSCAT deposits dust too quickly, and

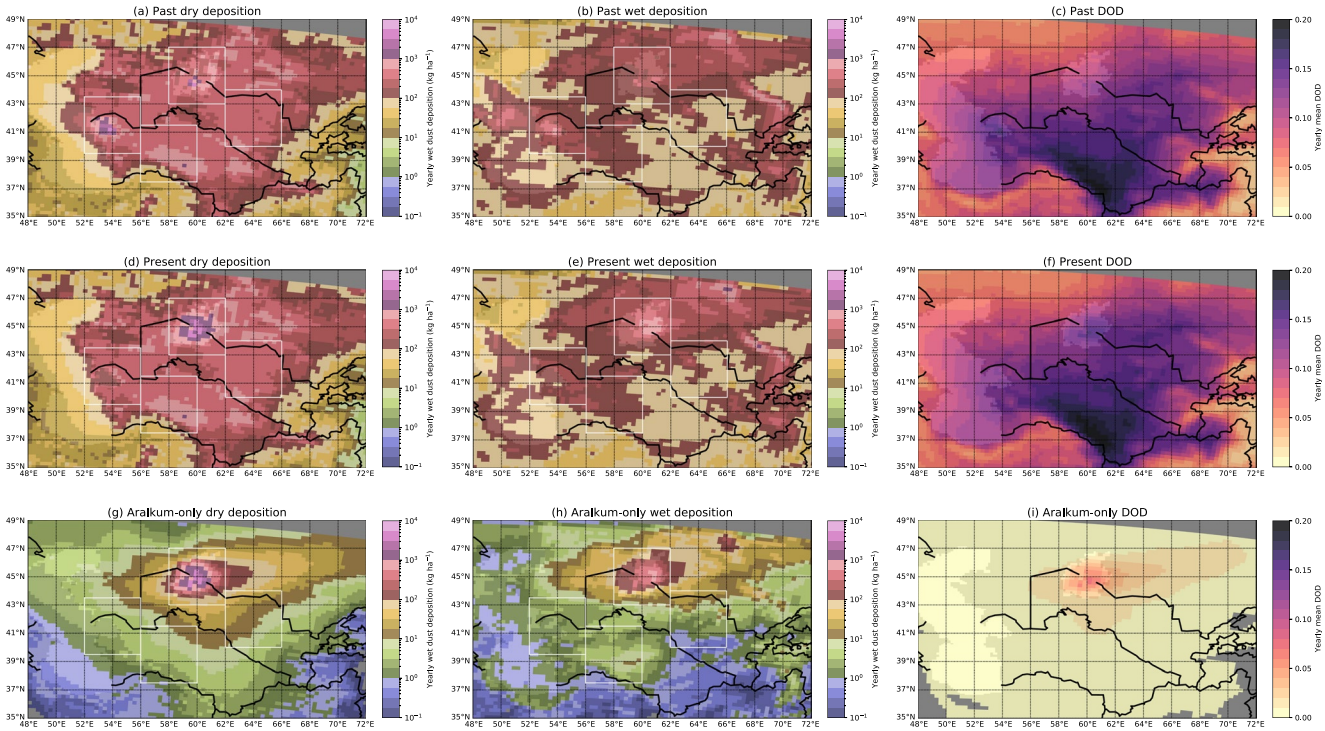

Figure 14. Maps of (a–c) past, (d–f) present, and (g–i) Aralkum-only dry and wet dust depositions and mean dust aerosol optical depths (DODs) over Central Asia during the course of the DUBLT simulation year. The four white boxes overlaid on the deposition maps indicate the four regions discussed in the text: the northern box is the Aralkum, the western box the Garabogazköl Basin, the southern box the Karakum, and the eastern box the Kyzylkum. Within the Aralkum box, the total deposition in the past is 8.5 Tg, the total in the present is 15.1 Tg, and the total in the Aralkum-only simulation is 8.9 Tg. Gray areas indicate grid cells either outside the domain (to the north-east), or areas with values below the color-scale threshold (panels (g–i) in the south).

that more dust is deposited closer to the source over the Aralkum itself: the maximum yearly dust deposition is 5,928 kg/ha in the grid cell at 44.59°N, 60.17°E, in the southern central Aralkum. Comparing this Aralkum grid cell with the sets of Aralkum and Kyzylkum measurements presented by Opp et al. (2019), it appears that the DUBLT scenario is to a limited extent able to reproduce the measured dust depositions, just not in precisely the same locations.

The impacts of dust deposition may also be relevant over agricultural land and over glaciers, both of which are landscapes found in Central Asia and which may be present downwind of the Aralkum. For example, dust deposited on snow and ice can accelerate the melting of the underlying snow and ice (Skiles et al., 2018), and may also be important for the water quality of Central Asian glaciers (Yapiyev et al., 2021). At Kazaly on the Syr Darya, during the year 591 kg/ha is deposited in the present simulation, of which 254 kg/ha is simulated by DUBLT_ARAL. In the Uzbek city of Nukus, situated to the south of the Aralkum and surrounded by agricultural land by the Amu Darya, 292 kg/ha is deposited of which 32 kg/ha comes from the Aralkum. As with air quality, it is clear that the agricultural land around the Syr Darya is more heavily influenced, to a substantial degree, by deposited dust from the Aralkum compared to other regions. As for the mountain regions, in the Pamir-Alay in northern Tajikistan 139 kg/ha is deposited, of which 3 kg/ha come from the Aralkum. This appears to be primarily due to wet deposition (Figures 14d, 14e, 14g, and 14h). While the other Central Asian deserts may be more substantial sources of dust deposited on the Pamir-Alay, the Aralkum still provides a contribution, and it is also clear that of the chains of mountains in the Tian Shan—Pamir—Himalayan region, it is the Pamir-Alay in the west that are the most influenced by Central Asian and Aralkum dust.

5. Conclusions

The Aralkum is a substantial anthropogenic contributor of dust to the atmospheric environment over Central Asia, a contribution which has grown steadily over the past six decades. Due to its relatively recent formation and also to its continuing growth, the Aralkum poses a challenge to modeling systems as to how to accurately represent

and understand the quantity of dust that it emits, and under what atmospheric and environmental conditions. This paper seeks to address this challenge by applying the Global Surface Water data set to the COSMO-MUSCAT aerosol transport model, so as to simulate the Central Asian dust life-cycle in two epochs during the Aralkum's formation and expansion, the 1980s–1990s (the "past") and the 2000s–2010s (the "present"). Making use of precise water coverage data in two epochs is a novel feature of this work, enabling the impact on the dust life-cycle solely due to changes in surface water coverage (exposing lakebed soils to aeolian erosion) to be discerned and analyzed on the inter-decadal timescale as well as on the Central Asian regional spatial scale. Furthermore, as a third sensitivity experiment, simulations of dust emitted only from the lakebed of the new Aralkum provide the novel capability to isolate the influence of the Aralkum on the regional dust life-cycle.

There are three key findings:

1. *The expanded lakebed of the Aralkum has contributed approximately an extra 7% to regional Central Asian dustiness over the past 30 years*. Between the 1980s and the 2010s, the Aralkum region has seen a near-doubling in its dust emissions as simulated by the DUBLT scenarios, from 14.3 Tg in the 1980s and 1990s to 27.1 Tg in the 2000s and 2010s. On the seasonal cycle, dust emissions from the Aralkum appear to peak in spring and early winter, albeit with the caveat that this is what is simulated within the case-study of a 1-year period. The bulk of these emissions (14.5 Tg out of 27.1 Tg) from March 2015 to March 2016 are driven by westerly winds, an unexpected result given the dominance of easterly and north-easterly winds in previous studies, such that regions and settlements directly to the east of the Aralkum are worst affected by dust originating from it, out to a distance as far as ∼600 km from the centre of the Aralkum. Of the major cities in the region, Tashkent and Ashgabat appear to be the most affected by its dust, with Aralkum dust breaching WHO air quality guidelines respectively on two and three days during the year, despite being ∼800 km and more from the centre of the Aralkum. These cities are however more frequently and more heavily influenced by the closer neighboring deserts of the Karakum and the Kyzylkum.
2. *Over two thirds of the Aralkum's dust events may not be observable by satellites*. The modeling approach to understanding the Aralkum's dust cycle highlights the apparently coincident nature of dust activity and cloud cover over the region. 18.5 of the 27.1 Tg of dust emitted by the Aralkum over the year are emitted under cloudy skies (cloud cover >95%), and hence would be impossible to observe using many remote sensing techniques, such as from satellites or from AERONET ground-based sun-photometers. This may also contribute to the explanation for the discrepancy in the dust transport pathways provided by the DUBLT scenario compared to previous observational studies: remote sensing methods may simply be unable to capture the full range of dust storm patterns from the Aralkum. Furthermore, as the comparisons with VIIRS show, satellite retrievals may often not be performed over the temporally variable surface of the Aralkum, further confounding the observational record. Getting a glimpse of that which may not be observable from satellites is an advantage of the modeling approach with respect to dust from the Aralkum, which also suggests targets (e.g., the influence on the regional radiation budget) for further combined modeling and ground-based observation studies in the region.
3. *There is a high degree of interannual variability in the direction of dust-producing high wind speed events over the Aralkum*. As revealed by ERA5 wind data, the surface wind patterns over the Aralkum and its neighboring deserts manifest a high degree of interannual variability, and so it has become clear that the directions in which Aralkum dust storms travel (and their intensity) will vary from year to year. Previous authors (e.g., Semenov, 2012) have observed a typical easterly and north-easterly wind pattern over the Aralkum during previous years in the early 21st century, however this pattern is not repeated during the DUBLT 2015–2016 1-year period. This variability would have consequences for which parts of the Central Asian region will be downwind of the Aralkum in a given year, so for example, while Tashkent and Ashgabat may be the major cities most influenced by Aralkum dust during the DUBLT simulation period, other cities in different directions may be worse affected during other years. There is clear scope for evolving atmospheric circulation patterns to have an impact on the life-cycle of dust emitted from the Aralkum, such that the patterns of dust behavior modeled during the DUBLT simulation period and measured during the previous decade will not always be present over the Aralkum. On the other hand, the patterns simulated during the DUBLT year may become more common as Arctic winter warming events become more frequent, causing shifts to the winter wind patterns in the Northern Hemisphere (e.g., Cohen et al., 2018) and driving more frequent westerly winds over the Aralkum. Much remains unclear however, and ongoing observations and modeling are required to confirm and describe the significance of this variability in wind patterns for the Aralkum's dust distribution.

Data Availability Statement

The COSMO-MUSCAT output relating to the DUBLT (present), DUBLT_PAST and DUBLT_ARAL simulations are publicly available on Zenodo (Banks et al., 2022). Global Surface Water data were provided by the European Commission's Joint Research Centre, part of the Copernicus Programme (Global Surface Water, 2016). SoilGrids version 2.0 data are provided by the International Soil Reference Information Centre (SoilGrids, 2020). MODIS monthly NDVI (MYD13C2) and 8-day snow cover (MYD10C2) data are provided by NASA (MODIS NDVI, 2015; MODIS Snow, 2016). ERA5 hourly data on single levels were provided by ECMWF (ERA5, 2018). CAMS aerosol reanalysis data were provided by Copernicus and ECMWF (CAMS, 2019). VIIRS/SNPP Deep Blue Level 3 daily aerosol retrieval data (AERDB_D3_VIIRS_SNPP) are available from NASA Goddard Space Flight Center (VIIRS AOD, 2018), as are AERONET data (AERONET, 1998). We acknowledge the use of Landsat and MODIS imagery from the NASA Worldview application (EOSDIS Worldview, 2016), part of the NASA Earth Observing System Data and Information System (EOSDIS). All webpages were last verified on 9 September 2022.

Acknowledgments
JRB has been funded for this work by the Deutsche Forschungsgemeinschaft (DFG), under the project DESERT-TIME (Grant BA 6612/1-1). Access to the COSMO model has been provided by Deutscher Wetterdienst (DWD), which also provided boundary data. The authors thank the PIs of the six AERONET sites used in this study for maintaining the sites and for providing the data. Finally, the authors thank Ron Miller, Maria Shahgedanova and a third reviewer for their constructive comments during the review process. Open Access funding enabled and organized by Projekt DEAL.

References

Abadi, A. R. S., Hamzeh, N. H., Shukurov, K., Opp, C., & Dumka, U. C. (2022). Long-term investigation of aerosols in the Urmia Lake region in the Middle East by ground-based and satellite data in 2000-2021. *Remote Sensing*, *14*(3827), 3827. https://doi.org/10.3390/rs14153827

AERONET. (1998). AERONET aerosol optical depth [Dataset]. NASA Goddard Space Flight Center. Retrieved from https://aeronet.gsfc.nasa.gov/

Alizadeh-Choubari, O., Zawar-Reza, P., & Sturman, A. (2014). The "wind of 120 days" and dust storm activity over the Sistan Basin. *Atmospheric Research*, *143*, 328–341. https://doi.org/10.1016/j.atmosres.2014.02.001

American Meteorological Society. (2022). Glossary of meteorology. Retrieved from https://glossary.ametsoc.org/wiki/Gust

Argaman, E., Singer, A., & Tsoar, H. (2006). Erodibility of some crust forming soils/sediments from the Southern Aral Sea Basin as determined in a wind tunnel. *Earth Surface Processes and Landforms*, *31*(1), 47–63. https://doi.org/10.1002/esp.1230

Banks, J. R., Brindley, H. E., Stenchikov, G., & Schepanski, K. (2017). Satellite retrievals of dust aerosol over the red sea and the Persian gulf. *Atmospheric Chemistry and Physics*, *17*(6), 3987–4003. https://doi.org/10.5194/acp-17-3987-2017

Banks, J. R., Heinold, B., & Schepanski, K. (2022). Dataset associated with Banks et al. (2022): Impacts of the desiccation of the Aral Sea on the Central Asian dust life-cycle [Dataset]. Zenodo. https://doi.org/10.5281/zenodo.6022747

Banks, J. R., Schepanski, K., Heinold, B., Hünerbein, A., & Brindley, H. E. (2018). The influence of dust optical properties on the colour of simulated msg-seviri desert dust infrared imagery. *Atmospheric Chemistry and Physics*, *18*(13), 9681–9703. https://doi.org/10.5194/acp-18-9681-2018

Breckle, S.-W., & Geldeyeva, G. V. (2012). Dynamics of the Aral Sea in geological and historical times. In S.-W. Breckle, W. Wucherer, L. A. Dimeyeva, & N. P. Ogar (Eds.), *Aralkum—A man-made desert: The desiccated floor of the Aral Sea (Central Asia)* (pp. 13–35). Springer.

Breckle, S.-W., & Wucherer, W. (2012). The Aralkum, a man-made desert on the desiccated floor of the Aral Sea (Central Asia): General introduction and aims of the book. In S.-W. Breckle, W. Wucherer, L. A. Dimeyeva, & N. P. Ogar (Eds.), *Aralkum—A man-made desert: The desiccated floor of the Aral Sea (Central Asia)* (pp. 1–9). Springer.

Buck, B. J., King, J., & Etyemezian, V. (2011). Effects of salt mineralogy on dust emissions, Salton Sea, California. *Soil Science Society of America Journal*, *75*(5), 1971–1985. https://doi.org/10.2136/sssaj2011.0049

Cakmur, R. V., Miller, R. L., & Torres, O. (2004). Incorporating the effect of small-scale circulations upon dust emission in an atmospheric general circulation model. *Journal of Geophysical Research*, *109*(D7), D07201. https://doi.org/10.1029/2003JD004067

CAMS. (2019). CAMS global reanalysis (EAC4) [Dataset]. Copernicus/ECMWF. Retrieved from https://ads.atmosphere.copernicus.eu/cdsapp#!/dataset/cams-global-reanalysis-eac4

Carroll, M. L., DiMiceli, C. M., Townshend, J. R. G., Sohlberg, R. A., Elders, A. I., Devadiga, S., et al. (2017). Development of an operational land water mask for MODIS Collection 6, and influence on downstream data products. *International Journal of Digital Earth*, *10*(2), 207–218. https://doi.org/10.1080/17538947.2016.1232756

Cohen, J., Pfeiffer, K., & Francis, J. A. (2018). Warm Arctic episodes linked with increased frequency of extreme winter weather in the United States. *Nature Communications*, *9*(869), 869. https://doi.org/10.1038/s41467-018-02992-9

Darmenova, K., & Sokolik, I. N. (2007). Assessing uncertainties in dust emission in the Aral Sea region caused by meteorological fields predicted with a mesoscale model. *Global and Planetary Change*, *56*(3–4), 297–310. https://doi.org/10.1016/j.gloplacha.2006.07.024

Darmenova, K., Sokolik, I. N., Shao, Y., Marticorena, B., & Bergametti, G. (2009). Development of a physically based dust emission module within the Weather Research and Forecasting (WRF) model: Assessment of dust emission parameterizations and input parameters for source regions in Central and East Asia. *Journal of Geophysical Research*, *114*(D14), D14201. https://doi.org/10.1029/2008JD011236

Didan, K. (2015). MYD13C2 MODIS/Aqua vegetation indices monthly L3 global 0.05Deg CMG V006 [CMG 0.05 Deg Monthly NDVI]. *NASA EOSDIS Land Processes DAAC*. https://doi.org/10.5067/MODIS/MYD13C2.006

Dubovik, O., Holben, B., Eck, T. F., Smirnov, A., Kaufman, Y. J., King, M. D., et al. (2002). Variability of absorption and optical properties of key aerosol types observed in worldwide locations. *Journal of the Atmospheric Sciences*, *59*(3), 590–608. https://doi.org/10.1175/1520-0469(2002)059<0590:voaaop>2.0.co;2

EOSDIS Worldview. (2016). Landsat and MODIS imagery [Dataset]. NASA Worldview. Retrieved from https://worldview.earthdata.nasa.gov/

ERA5. (2018). ERA5 hourly data on single levels from 1959 to present [Dataset]. Copernicus/ECMWF. Retrieved from https://cds.climate.copernicus.eu/cdsapp#!/dataset/reanalysis-era5-single-levels

Gasse, F. (2002). Diatom-inferred salinity and carbonate oxygen isotopes in Holocene waterbodies of the Western Sahara and Sahel (Africa). *Quaternary Science Reviews*, *21*(7), 737–767. https://doi.org/10.1016/S0277-3791(01)00125-1

Ge, Y., Abuduwaili, J., Ma, L., & Liu, D. (2016). Temporal variability and potential diffusion characteristics of dust aerosol originating from the Aral Sea Basin, Central Asia. *Water, Air, and Soil Pollution*, *227*(63), 63. https://doi.org/10.1007/s11270-016-2758-6

Gholampour, A., Nabizadeh, R., Hassanvand, M. S., Taghipour, H., Nazmara, S., & Mahvi, A. H. (2015). Characterization of saline dust emission resulted from Urmia Lake drying. *Journal of Environmental Health Science and Engineering*, *13*(82), 82. https://doi.org/10.1186/s40201-015-0238-3

Gillette, D., Ono, D., & Richmond, K. (2004). A combined modeling and measurement technique for estimating windblown dust emissions at Owens (dry) Lake, California. *Journal of Geophysical Research*, *109*(F1), F01003. https://doi.org/10.1029/2003JF000025

Global Surface Water. (2016). Global surface water [Dataset]. European Commission Joint Research Centre. Retrieved from https://global-surface-water.appspot.com/download

Graham, R. M., Cohen, L., Petty, A. A., Boisvert, L. N., Rinke, A., Hudson, S. R., et al. (2017). Increasing frequency and duration of Arctic winter warming events. *Geophysical Research Letters*, *44*(13), 6974–6983. https://doi.org/10.1002/2017GL073395

Groll, M., Opp, C., & Aslanov, I. (2013). Spatial and temporal distribution of the dust deposition in Central Asia—Results from a long term monitoring program. *Aeolian Research*, *9*, 49–62. https://doi.org/10.1016/j.aeolia.2012.08.002

Groll, M., Opp, C., Semenov, O., Issanova, G., & Shapov, A. (2021). Ground-based dust deposition monitoring in the Aral Sea basin. In E. Saljnikov, L. Mueller, A. Lavrishchev, & F. Eulenstein (Eds.), *Advances in understanding soil degradation* (pp. 229–243). Springer. https://doi.org/10.1007/978-3-030-85682-3_9

Hall, D. K., & Riggs, G. A. (2016). *MODIS/Aqua snow cover 8-day L3 global 0.05Deg CMG, version 6 [eight day CMG snow cover]*. NASA National Snow and Ice Data Center Distributed Active Archive Center. https://doi.org/10.5067/MODIS/MYD10C2.006

He, S., Xu, X., Furevik, T., & Gao, Y. (2020). Eurasian cooling linked to the vertical distribution of Arctic warming. *Geophysical Research Letters*, *47*(10), e2020GL087212. https://doi.org/10.1029/2020GL087212

Heinold, B., Tegen, I., Schepanski, K., Tesche, M., Essenborn, M., Freudenthaler, V., et al. (2011). Regional modelling of Saharan dust and biomass-burning smoke. Part 1: Model description and evaluation. *Tellus*, *63B*(4), 781–799. https://doi.org/10.1111/j.1600-0889.2011.00570.x

Helmert, J., Heinold, B., Tegen, I., Hellmuth, O., & Wendisch, M. (2007). On the direct and semidirect effects of saharan dust over Europe: A modeling study. *Journal of Geophysical Research*, *112*(D13), D13208. https://doi.org/10.1029/2006JD007444

Hengl, T., de Jesus, J. M., Heuvelink, G. B. M., Gonzalez, M. R., Kilibarda, M., Blagotic, A., et al. (2017). SoilGrids250m: Global gridded soil information based on machine learning. *PLoS One*, *12*(2), e0169748. https://doi.org/10.1371/journal.pone.0169748

Hersbach, H., Bell, B., Berrisford, P., Biavati, G., Horányi, A., Sabater, J. M., et al. (2018). ERA5 hourly data on single levels from 1979 to present. *Copernicus Climate Change Service (C3S) Climate Data Store (CDS)*. https://doi.org/10.24381/cds.adbb2d47

Hersbach, H., Bell, B., Berrisford, P., Hirahara, S., Horányi, A., Muñoz-Sabater, J., et al. (2020). The ERA5 global reanalysis. *Quarterly Journal of the Royal Meteorological Society*, *146*(730), 1999–2049. https://doi.org/10.1002/qj.3803

Hofer, J., Althausen, D., Abdullaev, S. F., Makhmudov, A. N., Nazarov, B. I., Schettler, G., et al. (2017). Long-term profiling of mineral dust and pollution aerosol with multiwavelength polarization Raman lidar at the Central Asian site of Dushanbe, Tajikistan: Case studies. *Atmospheric Chemistry and Physics*, *17*(23), 14559–14577. https://doi.org/10.5194/acp-17-14559-2017

Hofer, J., Ansmann, A., Althausen, D., Engelmann, R., Baars, H., Abdullaev, S. F., & Makhmudov, A. N. (2020). Long-term profiling of aerosol light extinction, particle mass, cloud condensation nuclei, and ice-nucleating particle concentration over Dushanbe, Tajikistan, in Central Asia. *Atmospheric Chemistry and Physics*, *20*(8), 4695–4711. https://doi.org/10.5194/acp-20-4695-2020

Holben, B. N., Eck, T. F., Slutsker, I., Tanré, D., Buis, J. P., Setzer, A., et al. (1998). AERONET- A federated instrument network and data archive for aerosol characterization. *Remote Sensing of Environment*, *66*(1), 1–16. https://doi.org/10.1016/S0034-4257(98)00031-5

Hsu, N. C., Lee, J., Sayer, A. M., Kim, W., Bettenhausen, C., & Tsay, S.-C. (2019). VIIRS deep blue aerosol products over land: Extending the EOS long-term aerosol data records. *Journal of Geophysical Research: Atmospheres*, *124*(7), 4026–4053. https://doi.org/10.1029/2018JD029688

Huneeus, N., Schulz, M., Balkanski, Y., Griesfeller, J., Prospero, J., Kinne, S., et al. (2011). Global dust model intercomparison in AeroCom phase I. *Atmospheric Chemistry and Physics*, *11*(15), 7781–7816. https://doi.org/10.5194/acp-11-7781-2011

Indoitu, R., Kozhoridze, G., Batyrbaeva, M., Vitkovskaya, I., Orlovsky, N., Blumberg, D., & Orlovsky, L. (2015). Dust emission and environmental changes in the dried bottom of the Aral Sea. *Aeolian Research*, *17*, 101–115. https://doi.org/10.1016/j.aeolia.2015.02.004

Inness, A., Ades, M., Agusti-Panareda, A., Barré, J., Benedictow, A., Blechschmidt, A.-M., et al. (2019). The CAMS reanalysis of atmospheric composition. *Atmospheric Chemistry and Physics*, *19*(6), 3515–3556. https://doi.org/10.5194/acp-19-3515-2019

Issanova, G., Abuduwaili, J., Galayeva, O., Semenov, O., & Bazarbayeva, T. (2015). Aeolian transportation of sand and dust in the Aral Sea region. *International journal of Environmental Science and Technology*, *12*(10), 3213–3224. https://doi.org/10.1007/s13762-015-0753-x

Kaplan, J. O. (2001). Geophysical applications of vegetation modeling (Unpublished doctoral dissertation). *Department of Ecology, Lund University*.

Karami, S., Hamzeh, N. H., Kaskaoutis, D. G., Rashki, A., Alam, K., & Ranjbar, A. (2021). Numerical simulations of dust storms originated from dried lakes in central and southwest Asia: The case of Aral Sea and Sistan Basin. *Aeolian Research*, *50*, 100679. https://doi.org/10.1016/j.aeolia.2021.100679

Kaskaoutis, D. G., Rashki, A., Houssos, E. E., Mofidi, A., Goto, D., Bartzokas, A., et al. (2015). Meteorological aspects associated with dust storms in the Sistan region, southeastern Iran. *Climate Dynamics*, *45*(1–2), 407–424. https://doi.org/10.1007/s00382-014-2208-3

Knorr, W., & Heimann, M. (1995). Impact of drought stress and other factors on seasonal land biosphere CO_2 exchange studied through an atmospheric tracer transport model. *Tellus B: Chemical and Physical Meteorology*, *47*(4), 471–489. https://doi.org/10.1034/j.1600-0889.47.issue4.7.x

Koren, I., Kaufman, Y. J., Washington, R., Todd, M. C., Rudich, Y., Martins, J. V., & Rosenfeld, D. (2006). The Bodélé depression: A single spot in the Sahara that provides most of the dust to the Amazon forest. *Environmental Research Letters*, *1*, 014005. https://doi.org/10.1088/1748-9326/1/1/014005

Levy, R. C., Mattoo, S., Sawyer, V., Shi, Y., Colarco, P. R., Lyapustin, A. I., et al. (2018). Exploring systematic offsets between aerosol products from the two MODIS sensors. *Atmospheric Measurement Techniques*, *11*(7), 4073–4092. https://doi.org/10.5194/amt-11-4073-2018

Li, L., & Sokolik, I. N. (2017). Developing a dust emission procedure for Central Asia. *Air, Soil and Water Research*, *10*, 1–12. https://doi.org/10.1177/1178622117711939

Li, L., & Sokolik, I. N. (2018). The dust direct radiative impact and its sensitivity to the land surface state and key minerals in the WRF-chem-DuMo model: A case study of dust storms in Central Asia. *Journal of Geophysical Research: Atmospheres*, *123*(9), 4564–4582. https://doi.org/10.1029/2017JD027667

Löw, F., Navratil, P., Kotte, K., Schöler, H. F., & Bubenzer, O. (2013). Remote-sensing-based analysis of landscape change in the desiccated seabed of the Aral Sea-a potential tool for assessing the hazard degree of dust and salt storms. *Environmental Monitoring and Assessment*, *185*(10), 8303–8319. https://doi.org/10.1007/s10661-013-3174-7

Lunt, D. J., & Valdes, P. J. (2002). The modern dust cycle: Comparison of model results with observations and study of sensitivities. *Journal of Geophysical Research*, *107*(D23), 4669. https://doi.org/10.1029/2002JD002316

Marticorena, B., & Bergametti, G. (1995). Modeling the atmospheric dust cycle: 1. Design of a soil-derived dust emission scheme. *Journal of Geophysical Research*, *100*(D8), 16415–16430. https://doi.org/10.1029/95jd00690
Marticorena, B., Bergametti, G., Aumont, B., Callot, Y., N'Doume, C., & Legrand, M. (1997). Modeling the atmospheric dust cycle: 2. Simulation of saharan dust sources. *Journal of Geophysical Research*, *102*(D4), 4387–4404. https://doi.org/10.1029/96jd02964
Menut, L., Pérez, C., Haustein, K., Bessagnet, B., Prigent, C., & Alfaro, S. (2013). Impact of surface roughness and soil texture on mineral dust emission fluxes modeling. *Journal of Geophysical Research: Atmosphere*, *118*(12), 6505–6520. https://doi.org/10.1002/jgrd.50313
Micklin, P. (2010). The past, present, and future Aral Sea. *Lakes and Reservoirs: Research and Management*, *15*(3), 193–213. https://doi.org/10.1111/j.1440-1770.2010.00437.x
Mie, G. (1908). Beiträge zur Optik trüber Medien speziell kolloidaler Metallösungen. *Annals of Physics*, *330*(3), 377–445. https://doi.org/10.1002/andp.19083300302
MODIS NDVI. (2015). MODIS monthly NDVI (MYD13C2) [Dataset]. NASA Earthdata. Retrieved from https://search.earthdata.nasa.gov/search
MODIS Snow. (2016). Modis 8-day snow (MYD10C2) [Dataset]. NASA Earthdata. Retrieved from https://search.earthdata.nasa.gov/search
Mohammadpour, K., Sciortino, M., Kaskaoutis, D. G., & Rashki, A. (2022). Classification of synoptic weather clusters associated with dust accumulation over southeastern areas of the Caspian Sea (Northeast Iran and Karakum desert). *Aeolian Research*, *54*, 100771. https://doi.org/10.1016/j.aeolia.2022.100771
Moore, G. W. K. (2016). The December 2015 north pole warming event and the increasing occurrence of such events. *Scientific Reports*, *6*(1), 39084. https://doi.org/10.1038/srep39084
Morcrette, J.-J., Mozdzynski, G., & Leutbecher, M. (2008). A reduced radiation grid for the ECMWF integrated forecasting system. *Monthly Weather Review*, *136*(12), 4760–4772. https://doi.org/10.1175/2008MWR2590.1
Nield, J. M., McKenna Neuman, C., O'Brien, P., Bryant, R. G., & Wiggs, G. F. S. (2016). Evaporative sodium salt crust development and its wind tunnel derived transport dynamics under variable climatic conditions. *Aeolian Research*, *23*, 51–62. https://doi.org/10.1016/j.aeolia.2016.09.003
Nobakht, M., Shahgedanova, M., & White, K. (2021). New inventory of dust emission sources in Central Asia and Northwestern China derived from MODIS imagery using dust enhancement technique. *Journal of Geophysical Research: Atmospheres*, *126*(4). https://doi.org/10.1029/2020JD033382
Notaro, M., Yu, Y., & Kalashnikova, O. V. (2015). Regime shift in Arabian dust activity, triggered by persistent Fertile Crescent drought. *Journal of Geophysical Research: Atmospheres*, *120*(19), 10229–10249. https://doi.org/10.1002/2015JD023855
O'Hara, S. L., Wiggs, G. F. S., Mamedov, B., Davidson, G., & Hubbard, R. B. (2000). Exposure to airborne dust contaminated with pesticide in the Aral Sea region. *The Lancet*, *355*(9204), 627–628. https://doi.org/10.1016/S0140-6736(99)04753-4
Opp, C., Groll, M., Aslanov, I., Lotz, T., & Vereshagina, N. (2017). Aeolian dust deposition in the southern Aral Sea region (Uzbekistan): Ground-based monitoring results from the LUCA project. *Quaternary International*, *429*, 86–99. https://doi.org/10.1016/j.quaint.2015.12.103
Opp, C., Groll, M., Semenov, O., Vereshagina, N., & Khamzina, A. (2019). Impact of the Aral Sea syndrome—The Aralkum as a man-made dust source. *E3S Web of Conferences*, *99*, 03003. https://doi.org/10.1051/e3sconf/20199903003
Overland, J. E., Kim, B.-M., & Tachibana, Y. (2021). Communicating Arctic-midlatitude weather and ecosystem connections: Direct observations and sources of intermittency. *Environmental Research Letters*, *16*(10), 105006. https://doi.org/10.1088/1748-9326/ac25bc
Pekel, J.-F., Cottam, A., Gorelick, N., & Belward, A. S. (2016). High-resolution mapping of global surface water and its long-term changes. *Nature*, *540*(7633), 418–422. https://doi.org/10.1038/nature20584
Poggio, L., de Sousa, L. M., Batjes, N. H., Heuvelink, G. B. M., Kempen, B., Ribeiro, E., & Rossiter, D. (2021). SoilGrids 2.0: Producing soil information for the globe with quantified spatial uncertainty. *SOIL*, *7*(1), 217–240. https://doi.org/10.5194/soil-7-217-2021
Prigent, C., Jiménez, C., & Catherinot, J. (2012). Comparison of satellite microwave backscattering (ASCAT) and visible/near-infrared reflectances (PARASOL) for the estimation of aeolian aerodynamic roughness length in arid and semi-arid regions. *Atmospheric Measurement Techniques*, *5*(11), 2703–2712. https://doi.org/10.5194/amt-5-2703-2012
Rashki, A., Kaskaoutis, D. G., Goudie, A. S., & Kahn, R. A. (2013). Dryness of ephemeral lakes and consequences for dust activity: The case of the Hamoun drainage basin, southeastern Iran. *Science of the Total Environment*, *463–464*, 552–564. https://doi.org/10.1016/j.scitotenv.2013.06.045
Rupakheti, D., Kang, S., Bilal, M., Gong, J., Xia, X., & Cong, Z. (2019). Aerosol optical depth climatology over Central Asian countries based on Aqua-MODIS Collection 6.1 data: Aerosol variations and sources. *Atmospheric Environment*, *207*, 205–214. https://doi.org/10.1016/j.atmosenv.2019.03.020
Sayer, A. M., Hsu, N. C., Bettenhausen, C., Lee, J., Kim, W. V., & Smirnov, A. (2018). Satellite ocean aerosol retrieval (SOAR) algorithm extension to S-NPP VIIRS as part of the "Deep Blue" aerosol project. *Journal of Geophysical Research: Atmospheres*, *123*(1), 380–400. https://doi.org/10.1029/2017JD027412
Sayer, A. M., Hsu, N. C., Lee, J., Kim, W. V., & Dutcher, S. T. (2019). Validation, stability, and consistency of MODIS collection 6.1 and VIIRS Version 1 deep blue aerosol data over land. *Journal of Geophysical Research: Atmospheres*, *124*(8), 4658–4688. https://doi.org/10.1029/2018JD029598
Schättler, U., Doms, G., & Schraff, C. (2014). A description of the nonhydrostatic regional COSMO-model, Part VII: User's guide (Tech. Rep.). *Deutscher Wetterdienst*. Retrieved from http://www.cosmo-model.org/
Schepanski, K., Heinold, B., & Tegen, I. (2017). Harmattan, saharan heat low, and West African monsoon circulation: Modulations on the saharan dust outflow towards the North Atlantic. *Atmospheric Chemistry and Physics*, *17*, 10223–10243. https://doi.org/10.5194/acp-17-10223-2017
Schulz, J.-P., & Heise, E. (2003). A new scheme for diagnosing near-surface convective gusts. *Consortium for Small-scale Modeling Newsletters*, *3*, 221–225. Retrieved from http://www.cosmo-model.org
Semenov, O. E. (2012). Dust storms and sandstorms and aerosol long-distance transport. In S.-W. Breckle, W. Wucherer, L. A. Dimeyeva, & N. P. Ogar (Eds.), *Aralkum—A man-made desert: The desiccated floor of the Aral Sea (Central Asia)* (pp. 73–82). Springer.
Sharifikia, M. (2013). Environmental challenges and drought hazard assessment of Hamoun Desert Lake in Sistan region, Iran, based on the time series of satellite imagery. *Natural Hazards*, *65*(1), 201–217. https://doi.org/10.1007/s11069-012-0353-8
Shi, W., Wang, M., & Guo, W. (2014). Long-term hydrological changes of the Aral Sea observed by satellites. *Journal of Geophysical Research: Oceans*, *119*(6), 3313–3326. https://doi.org/10.1002/2014JC009988
Sinyuk, A., Torres, O., & Dubovik, O. (2003). Combined use of satellite and surface observations to infer the imaginary part of refractive index of Saharan dust. *Geophysical Research Letters*, *30*(2). https://doi.org/10.1029/2002GL016189
Skiles, S. M., Flanner, M., Cook, J. M., Dumont, M., & Painter, T. H. (2018). Radiative forcing by light-absorbing particles in snow. *Nature Climate Change*, *8*(11), 964–971. https://doi.org/10.1038/s41558-018-0296-5
SoilGrids. (2020). Soilgrids250m Version 2.0 [Dataset]. ISRIC World Soil Information. Retrieved from https://soilgrids.org/

Soil Science Division Staff. (2017). Soil survey manual. In C. Ditzler, K. Scheffe, & H. C. Monger (Eds.), *USDA handbook 18*. Government Printing Office.

Sotoudeheian, S., Salim, R., & Arhami, M. (2016). Impact of middle eastern dust sources on PM_{10} in Iran: Highlighting the impact of Tigris-Euphrates basin sources and Lake Urmia desiccation. *Journal of Geophysical Research: Atmospheres*, *121*(23), 14018–14034. https://doi.org/10.1002/2016JD025119

Sternberg, T., & Edwards, M. (2017). Desert dust and health: A Central Asian review and steppe case study. *International Journal of Environmental Research and Public Health*, *14*(1342), 1342. https://doi.org/10.3390/ijerph14111342

Tegen, I., Harrison, S. P., Kohfeld, K., Prentice, I. C., Coe, M., & Heimann, M. (2002). Impact of vegetation and preferential source areas on global dust aerosol: Results from a model study. *Journal of Geophysical Research*, *107*(D21), AAC-14-1–AAC-14-27. https://doi.org/10.1029/2001JD000963

Todd, M. C., Washington, R., Martins, J. V., Dubovik, O., Lizcano, G., M'Bainayel, S., & Engelstaedter, S. (2007). Mineral dust emission from the Bodélé depression, northern Chad, during BoDEx 2005. *Journal of Geophysical Research*, *112*(D6), D06207. https://doi.org/10.1029/2006JD007170

Tourian, M. J., Elmi, O., Chen, Q., Devaraju, B., Roohi, S., & Sneeuw, N. (2015). A spaceborne multisensor approach to monitor the desiccation of Lake Urmia in Iran. *Remote Sensing of Environment*, *156*, 349–360. https://doi.org/10.1016/j.rse.2014.10.006

VIIRS AOD. (2018). VIIRS deep blue level 3 daily aerosol data (AERDB_D3_VIIRS_SNPP) [Dataset]. NASA Goddard Space Flight Center. Retrieved from https://ladsweb.modaps.eosdis.nasa.gov/search/

Washington, R., Todd, M. C., Lizcano, G., Tegen, I., Flamant, C., Koren, I., et al. (2006). Links between topography, wind, deflation, lakes and dust: The case of the Bodélé Depression, Chad. *Geophysical Research Letters*, *33*(9), L09401. https://doi.org/10.1029/2006gl025827

Wiggs, G. F. S., O'Hara, S. L., Wegerdt, J., van der Meers, J., Small, I., & Hubbard, R. (2003). The dynamics and characteristics of aeolian dust in dryland Central Asia: Possible impacts on human exposure and respiratory health in the Aral Sea basin. *The Geographical Journal*, *169*(2), 142–157. https://doi.org/10.1111/1475-4959.04976

Wolke, R., Schröder, W., Schrödner, R., & Renner, E. (2012). Influence of grid resolution and meteorological forcing on simulated European air quality: A sensitivity study with the modeling system COSMO-MUSCAT. *Atmospheric Environment*, *53*, 110–130. https://doi.org/10.1016/j.atmosenv.2012.02.085

World Health Organization (2021). *WHO global air quality guidelines: Particulate matter (PM2.5 and PM10), ozone, nitrogen dioxide, sulfur dioxide and carbon monoxide: Executive summary*. World Health Organization. Retrieved from https://apps.who.int/iris/handle/10665/345334

Wu, C., Lin, Z., & Liu, X. (2020). The global dust cycle and uncertainty in CMIP5 (Coupled Model Intercomparison Project phase 5) models. *Atmospheric Chemistry and Physics*, *20*(17), 10401–10425. https://doi.org/10.5194/acp-20-10401-2020

Xi, X., & Sokolik, I. N. (2016a). Dust interannual variability and trend in Central Asia from 2000 to 2014 and their climatic linkages. *Journal of Geophysical Research: Atmospheres*, *120*(23), 12175–12197. https://doi.org/10.1002/2015JD024092

Xi, X., & Sokolik, I. N. (2016b). Quantifying the anthropogenic dust emission from agricultural land use and desiccation of the Aral Sea in Central Asia. *Journal of Geophysical Research: Atmospheres*, *121*(20), 12270–12281. https://doi.org/10.1002/2016JD025556

Yapiyev, V., Wade, A. J., Shahgedanova, M., Saidaliyeva, Z., Madibekov, A., & Severskiy, I. (2021). The hydrochemistry and water quality of glacierized catchments in Central Asia: A review of the current status and anticipated change. *Journal of Hydrology: Regional Studies*, *38*, 100960. https://doi.org/10.1016/j.ejrh.2021.100960

Yu, Y., Notaro, M., Kalashnikova, O. V., & Garay, M. J. (2016). Climatology of summer Shamal wind in the Middle East. *Journal of Geophysical Research: Atmospheres*, *121*(1), 289–305. https://doi.org/10.1002/2015JD024063

Zängl, G., Reinert, D., Rípodas, P., & Baldauf, M. (2015). The ICON (ICOsahedral Non-hydrostatic) modelling framework of DWD and MPI-M: Description of the non-hydrostatic dynamical core. *Quarterly Journal of the Royal Meteorological Society*, *141*(687), 563–579. https://doi.org/10.1002/qj.2378